Arf GTPase activates the WAVE Regulatory Complex through a novel binding site

Sheng Yang[1], Yijun Liu[1], Abbigale Brown[1], Matthias Schaks[2,3,4], Bojian Ding[5], Daniel A. Kramer[1], Li Ding[6], Olga Alekhina[6], Daniel D. Billadeau[6], Saikat Chowdhury[5,7,8], Junmei Wang[9], Klemens Rottner[2,3,10], Baoyu Chen[1*]

Affiliations:

[1]Roy J. Carver Department of Biochemistry, Biophysics & Molecular Biology, Iowa State University, 2437 Pammel Drive, Ames, IA 50011, USA.

[2]Division of Molecular Cell Biology, Zoological Institute, Technische Universität Braunschweig, Spielmannstrasse 7, 38106 Braunschweig, Germany.

[3]Department of Cell Biology, Helmholtz Centre for Infection Research, Inhoffenstrasse 7, 38124 Braunschweig, Germany.

[4]Present address: Soilytix GmbH, Dammtorwall 7A, 20354 Hamburg, Germany

[5]Department of Biochemistry and Cell Biology, Stony Brook University, 100 Nicolls Road, Stony Brook, NY 11794, USA.

[6]Division of Oncology Research, College of Medicine, Mayo Clinic, Rochester MN, 55905

[7]CSIR-Centre for Cellular and Molecular Biology, Hyderabad, Telangana 500007, India

[8]Academy of Scientific and Innovative Research (AcSIR), Ghaziabad, Uttar Pradesh 201002, India

[9]Department of Pharmaceutical Sciences and Computational Chemical Genomics Screening Center, School of Pharmacy, University of Pittsburgh, 3501 Terrace St Pittsburgh, PA 15261, USA.

[10]Braunschweig Integrated Centre of Systems Biology (BRICS), Rebenring 56, 38106 Braunschweig, Germany.

[*]Correspondence: stone@iastate.edu

Summary

Crosstalk between Rho- and Arf-family GTPases plays an important role in linking actin cytoskeletal remodeling to membrane protrusion, organelle structure, and vesicle trafficking. The central actin regulator, WAVE Regulatory Complex (WRC), is a converging point of Rac1 (a Rho-family GTPase) and Arf signaling in many processes, but how Arf promotes WRC activation is unknown. Here we reconstituted a direct interaction between Arf and WRC. This interaction can be greatly enhanced by Rac1 binding to the D site of the WRC. Arf1 binds to a newly identified conserved surface on Sra1 located between the D site and the WH2 helix of WAVE1, which can drive WRC activation using a mechanism distinct from that of Rac1. Mutating Arf binding site abolishes Arf1-WRC interaction, disrupts Arf1-mediated WRC activation, and impairs lamellipodia morphology. This work uncovers a new mechanism underlying WRC activation and provides a mechanistic foundation for studying how WRC-mediated actin polymerization links Arf and Rac signaling in the cell.

Keywords

Arf1, Rac1, GTPase, Wiskott-Aldrich Syndrome protein, WAVE Regulatory Complex, WRC, actin, Arp2/3, lamellipodia

Introduction

Small GTPases of the Ras superfamily control diverse processes throughout eukaryotic cells (Wennerberg et al., 2005). Among them, the distantly related Arf-family and Rho-family GTPases play distinct roles and yet have extensive crosstalk in many different processes. Arf GTPases are key players in various steps of membrane trafficking and organelle morphogenesis, where they are best known to promote the assembly of coat proteins to initiate vesicle formation (D'Souza-Schorey and Chavrier, 2006; Donaldson and Jackson, 2011; Gillingham and Munro, 2007; Sztul et al., 2019). Rho GTPases, such as Rac1, are central regulators of the actin cytoskeleton in the formation of various cell membrane protrusions, such as lamellipodia and filopodia, where they are best known to promote cell migration, adhesion, and endocytosis (Etienne-Manneville and Hall, 2002; Mosaddeghzadeh and Ahmadian, 2021). Since it was discovered over two decades ago (Boshans et al., 2000; D'Souza-Schorey et al., 1997; Radhakrishna et al., 1999; Santy and Casanova, 2001), the crosstalk between Arf- and Rac1-mediated signaling pathways has been recognized as an essential component for the regulation of actin cytoskeletal dynamics during cell migration, spreading, adhesion, fusion, phagocytosis, and endocytosis (Boshans et al., 2000; Chen et al., 2003; D'Souza-Schorey et al., 1997; Hunt et al., 2022; Myers and Casanova, 2008; Phuyal and Farhan, 2019; Radhakrishna et al., 1999; Santy and Casanova, 2001; Singh et al., 2017). Nevertheless, our knowledge of the underlying molecular mechanism remains fragmental.

In addition to the role of Arf in regulating phospholipid microenvironment (Honda et al., 1999; Krauss et al., 2003), endosomal recycling of Rac1 (Balasubramanian et al., 2007; Boshans et al., 2000; Radhakrishna et al., 1999), and the localization and activity of

Rac1 GEFs (Chen et al., 2003; Koo et al., 2007; Palacios et al., 2002; Santy et al., 2005), GAPs(Hu et al., 2009), and adaptors (D'Souza-Schorey et al., 1997; Tarricone et al., 2001), a plethora of studies have underscored the convergence of Arf and Rac1 on a central actin nucleation promotion factor known as the WAVE Regulatory Complex (WRC) in many processes (Humphreys et al., 2012b, 2012a, 2013, 2016; Koronakis et al., 2011; Lewis-Saravalli et al., 2013; Marchesin et al., 2015; Singh et al., 2019, 2020). The WRC is a 400-kDa protein assembly containing five conserved proteins: Sra1 (or Cyfip2), Nap1 (or Hem1), Abi2 (or Abi1, Abi3), HSPC300, and WAVE1 (or WAVE2, WAVE3, members of the Wiskott-Aldrich Syndrome protein family). In the basal state, the WRC keeps WAVE auto-inhibited in the cytosol by sequestering the WCA (WH2-central-acidic) sequence at the C-terminus of WAVE through a collection of interactions with the Sra1 subunit and the "meander" sequence of WAVE (**Figure 1**, cartoon) (Chen et al., 2014a, 2010; Derivery et al., 2009; Eden et al., 2002; Ismail et al., 2009). Various membrane ligands can directly interact with and recruit the WRC to the plasma membrane and simultaneously activate it to release the WCA, which in turn can bind the Arp2/3 complex to polymerize branched actin filaments (Chen et al., 2014b, 2017; Koronakis et al., 2011; Lebensohn and Kirschner, 2009; Padrick et al., 2008; Rottner et al., 2021; Takenawa and Suetsugu, 2007; Zou et al., 2018). Among these ligands, Rac1 is the canonical activator of the WRC (Rottner et al., 2021). It acts by directly binding to two distinct locations on the opposite ends of the Sra1 subunit, which are named A and D sites, respectively. The two sites have ~40-fold difference in the affinity for Rac1 (Chen et al., 2017, 2010). The recent cryo-EM structures revealed that Rac1 binding to the low affinity site (A site), but not the

high-affinity site (D site), drives a conformational change to allosterically destabilize the WCA leading to WRC activation (Ding et al., 2022).

The connection between Arf1, Rac1 and the WRC was initially discovered by proteomic and cellular studies to identify proteins important for clathrin-AP-1-coated carrier biogenesis at the trans-Golgi network (TGN) (Anitei et al., 2010; Baust et al., 2006). A more direct connection was established in a seminal study by Koronakis and colleagues in 2011, in which they reconstituted WRC activation using lipid-coated beads and mammalian brain lysates (Koronakis et al., 2011). They found lipid-coated beads containing individual Rac1 or Arf1 only bound and activated WRC weakly, but beads containing both GTPases dramatically enhanced WRC membrane recruitment and activation (Koronakis et al., 2011). After that, a series of studies further corroborated the connection of Arf to the WRC. For example, Arf79 (the Arf1 homolog in *Drosophila*) was found to be critical for Sra1 localization and concomitant formation of lamellipodia (Humphreys et al., 2012a). This function could not be complemented by Rac overexpression, but could be restored by expressing the human Arf1, underlining the importance of Arf1 to WRC activation and the conserved role of the Arf-WRC interaction across species (Humphreys et al., 2012a). Furthermore, two different types of bacterial pathogens, *Salmonella enterica* and enteropathogenic and enterohemorrhagic *Escherichia coli* (EPEC and EHEC), could both hijack the Arf1-Rac1-WRC signaling axis to facilitate infection, albeit with opposite objectives (from the bacteria point of view) and via distinct mechanisms (Humphreys et al., 2012b, 2013, 2016). In addition, the cooperative actions of Arf1 (or Arf6) and Rac1 on the WRC were found to be critical for the migration of invasive MDA-MB-231 breast cancer cells (Lewis-Saravalli et al., 2013; Marchesin et al., 2015).

Moreover, a missense mutation in *Hem1* from patients with an inherited immunologic syndrome named immunodeficiency-72 with an autoinflammation (IMD72) was found to disrupt Arf1-, but not Rac1-mediated WRC activation (Cook et al., 2020).

Despite the importance of Arf1-Rac1-WRC signaling in various normal and disease-related processes, the mechanism by which Arf1 achieves this function is unknown. Sharing less than 30% sequence identity with Rac1, Arf1 may use a distinct mechanism to regulate the WRC. But does Arf1 directly interact with the WRC or Rac1 at all? If yes, what is the interaction mechanism, and what is the biochemical and structural basis of the cooperativity between Arf1 and Rac1? To answer these questions, here we have reconstituted a direct interaction between Arf and the WRC in solution by using purified proteins. We find the interaction is greatly enhanced by Rac1 binding to the WRC mainly on the D site. Remarkably, once bound to the WRC, Arf1 can directly activate the WRC independent of Rac1 binding to the A site. We further identified the Arf1 binding site, which is located at a conserved surface on Sra1 between the D site and the W helix of the WCA domain of WAVE. Mutating the Arf1 binding site abolished Arf1 binding, disrupted Arf1-mediated WRC activation, and impaired lamellipodia morphology. Together, our work reveals a new mechanism underlying WRC activation and paves the way for understanding how WRC-mediated actin polymerization integrates signals from Arf and Rac in various processes.

Results

Arf GTPases directly interact with WRC, and the interaction is greatly enhanced by Rac1

The interaction between Arf1 and WRC was initially discovered using lipid-coated beads where both Arf1 and Rac1 were anchored on the membrane and incubated with mammalian brain extracts (Koronakis et al., 2011). To examine if the Arf1-WRC interaction is direct and, if yes, to determine the underlying mechanism, we reconstituted this interaction in solution using recombinantly purified proteins. We found that GST-tagged Arf1 could directly pull down both the full-length (FL) WRC and a truncated WRC named ΔWRC230 (**Figure 1A**, lane 4, 10) (Chen et al., 2014a, 2017). ΔWRC230 represents the minimal, structured core of the WRC, since it lacks the C-terminal unstructured proline-rich region (PRR) and the WCA sequence of WAVE1, as well as the unstructured PRR and the SH3 domain of Abi2 (**Figure 1A**, cartoon). Although the binding signals were weak, they were specific in comparison to the background signals in GST controls (**Figure 1A**, lane 2 vs. 4, lane 7 vs. 10). Thus, Arf1 directly interacts with the WRC, and the structured core of the WRC is sufficient to bind Arf1.

To test if and how Rac1 can enhance Arf1 binding to the WRC, we used a Rac1 that contained two mutations, Q61L and P29S, which greatly enhanced Rac1 binding to the WRC as shown in our previous studies (Chen et al., 2017). Unless otherwise noted, we refer to this $Rac1^{Q61L/P29S}$ construct as Rac1 or $Rac1^{QP}$ interchangeably in this study. We found including free Rac1 in the pull-down reactions drastically enhanced GST-Arf1 binding to the WRC (**Figure 1A**, lane 6, 9). Note that Rac1 did not directly interact with Arf1 (**Figure 1A**, lane 5), but was co-retained with WRC by GST-Arf1 (**Figure 1A**, lane

6, 9). These results suggest that Arf1 and Rac1 can simultaneously bind to the same WRC via non-overlapping binding sites, and that Rac1 binding greatly stabilizes Arf1 binding.

As molecular switches, GTPases usually use the GTP state to engage with downstream effector proteins. We found that the Arf1-WRC interaction was also dependent on the nucleotide state of Arf1. Only Arf1 loaded with GTP, but not GDP, showed robust binding (**Figure 1B**, lane 4 vs. 5). Moreover, the interaction could be specifically blocked by EspG, a bacterial effector protein secreted into the host cell by enteropathogenic (EPEC) and enterohaemorrhagic (EHEC) *Escherichia coli* during infection (Dong et al., 2012; Humphreys et al., 2016). EspG directly binds the GTP-form of Arf1 and Arf6 (Dong et al., 2012; Humphreys et al., 2016) (also see **Figure 1B**, lane 1-3). This interaction was suggested to disrupt Arf-WRC signaling in host cells, which helped these extracellular pathogens evade WRC-mediated phagocytosis (Humphreys et al., 2016). Our data suggest EspG can achieve this by directly competing off Arf1 (and/or Arf6) binding to the WRC. Therefore, Arf1 may use the same surface to interact with the WRC and EspG.

We next used our previously established equilibrium pull-down (EPD) assay to quantitatively measure the enhancement of Arf1 binding by Rac1 (Chen et al., 2017; Pollard, 2010) (**Figure 1C**). We found that in the absence of Rac1, the Arf1-WRC interaction was weak, with a dissociate constant K_D ~23 μM (**Figure 1C**, black). By contrast, in the presence of 100 μM Rac1, which should saturate both A and D sites of the WRC (Chen et al., 2017; Ding et al., 2022), Arf1 binding affinity was increased nearly 30 fold (K_D ~ 0.66 μM, **Figure 1C**, orange). The enhanced binding was not an artifact of high concentration of free Rac1 included in the assay, as a mutant Rac1, in which the entire

Switch I motif critical for WRC binding was removed (herein referred to as $Rac1^{Dead}$; **Figure S1A**), could not promote Arf1 binding at the same concentration (**Figure 1C**, blue). Thus, Rac1 can enhance the weak interaction between Arf1 and WRC by ~30 fold.

We found Arf1 binding was likely mediated by the Sra1 or Nap1 subunit, but not WAVE1, Abi2 or HSPC300, as only the dimeric subcomplex containing Sra1/Nap1, but not the trimeric subcomplex formed by WAVE1/Abi2/HSPC300, showed weak binding signals comparable to the fully assembled, pentameric WRC (**Figure 1D**, lane 4 vs. 6, asterisks). Unlike binding to the intact WRC, however, the interaction with the Sra1/Nap1 dimer could not be enhanced by Rac1 (**Figure 1D**, lane 5 vs. 7, asterisks), suggesting that even though Sra1 or Nap1 may contain the Arf1 binding site, the enhancement of Arf1 binding by Rac1 is dependent on the fully assembled WRC. Moreover, we found that Arf1 binding to WRC was sensitive to both pH and salt concentration, with pH 6-7 and 50 mM NaCl, but not pH 8 or 100 mM NaCl being able to sustain the binding (**Figure 1E**, lane 2, 6). This indicates that the Arf-WRC binding involves polar interactions (see below).

We further tested if the Arf1-WRC interaction is unique to Arf1 or is general to other Arf-family proteins. In mammals, the Arf family contains six canonical members (Arf1-Arf6) and various distantly related Arf-like proteins (Arl) (Gillingham and Munro, 2007; Sztul et al., 2019). Based on sequence similarities, Arf1-Arf6 can be further divided into three classes: Class I (Arf1, 2, 3), Class II (Arf4, 5) and Class III (Arf6). We found that besides Arf1, Arf5 and Arf6 also robustly bound the WRC in a Rac1-dependent manner, although perhaps with slightly different affinities (**Figure 1F**, lane 1-6). By contrast, Arl1 or Arl2 did not show clear binding (**Figure 1F**, lane 7-10). These results suggest that the six members of Arf family, but perhaps not the more divergent Arl proteins,

can use the same mechanism to interact with the WRC. Together, our biochemical reconstitution established a direct, nucleotide-dependent interaction between Arf-family GTPases and WRC. This interaction is greatly enhanced by Rac1 binding to the WRC.

Arf1 binding mainly depends on Rac1 binding to the D site

Rac1 can bind to both the A and D sites on WRC, albeit with distinct affinities and effects on WRC activation (Chen et al., 2017; Ding et al., 2022). Therefore, we asked which Rac1 binding event was key to promoting Arf1 binding. To answer this question, we first used single amino acid mutations to specifically disrupt the A or D site from binding to Rac1 (Chen et al., 2017, 2010; Ding et al., 2022) (**Figure 2A**, cartoon). When Rac1 binding to the A site was disrupted by Sra1^{C179R}, Rac1 binding to the D site still enhanced Arf1 binding, but to a lower extent than the WT WRC (**Figure 2A**, lane 6, 7). By contrast, when Rac1 binding to the D site was disrupted by Sra1^{Y967A}, Rac1 binding to the A site could no longer promote Arf1 binding (**Figure 2A**, lane 8, 9). These data indicate that Rac1 binding to the D site plays a more important role in promoting Arf1 binding.

To further validate this result, we used EPD assays to directly measure the binding affinities of Arf1 to WRCs with disrupted A vs. D site. For this, instead of using the above single amino acid mutations to disrupt either site, which may retain weak, residual Rac1-binding activity, we inserted an inert protein PGS (glycogen synthase from the extreme thermophile *Pyrococcus abysii*) to a surface loop at the A or D site to completely block Rac1 binding. We herein name the new variants WRC$^{A\text{-block}}$ and WRC$^{D\text{-block}}$, respectively (**Figure 2B**, cartoon). Being a small, stable protein and with its N- and C- termini located in close proximity (6.5 Å), PGS was initially used to insert into the human

orexin/hypocretin receptors hOX1R and hOX2R to stabilize an intracellular loop and produce high-resolution diffracting crystals (Yin et al., 2015, 2016). Inserting PGS into the surface loop of the A or D site did not affect WRC assembly or purification (**Figure S2A, B**) or the basal level of Arf1-WRC interaction in the absence of free Rac1 (**Figure S1C**), but indeed further reduced the affinity measurement of Rac1 to WRC (from K_D ~ 2 μM for WRC^{Y967A} to ~7.5 μM for $WRC^{D\text{-}block}$; **Figure S1B**, blue vs. orange), likely due to eliminating the residual Rac1 binding to the D site in WRC^{Y967A}. When we blocked the A site and subjected the D site to 100 μM Rac1, Arf1 binding was enhanced, although not to the level of WT WRC (K_D ~5.76 μM for $WRC^{A\text{-}block}$ vs. ~0.66 μM for the WT WRC; **Figure 2B**, purple vs. orange; **Figure S1D**), suggesting Rac1 binding to the D site was partially sufficient to promote Arf1 binding. By contrast, when we blocked the D site and exposed the A site to 100 μM Rac1, Arf1 binding was not enhanced, but remained similar to that in the absence of Rac1 or in the presence of 100 μM $Rac1^{Dead}$ (K_D ~38.8 μM; **Figure 2B**, blue; **Figure 1C**, black; **Figure S1C**, orange), suggesting Rac1 binding to the A site alone could not promote Arf1 binding in this specific experimental condition (but see below).

As an alternative strategy to validate the contribution of the D site to Arf1 binding, we stabilized Rac1 binding to the D site by tethering it to the C-terminus of Sra1 (which we refer to as $\Delta WRC230^{D\text{-}Rac1}$) (Ding et al., 2022) or the C-terminus of WAVE1 that lacked the WCA (which we named $\Delta WRC230^{WAVE1\text{-}Rac1}$) (Chen et al., 2017) (**Figure 2C**, cartoon). These constructs stabilize D site Rac1 binding, which had allowed us to solve cryo-EM structures of the WRC with Rac1 bound to the D site (Chen et al., 2017; Ding et al., 2022). We found that, without free Rac1, both $\Delta WRC230^{D\text{-}Rac1}$ and $\Delta WRC230^{WAVE1\text{-}Rac1}$ were

able to enhance Arf1 binding to the level of the WT WRC enhanced by free Rac1 (**Figure 2C**, lane 4, 5, 7). Furthermore, in the EPD assay, ΔWRC230$^{D\text{-}Rac1}$ without free Rac1 enhanced Arf1 binding to a level nearly identical to that of the WRC$^{A\text{-}block}$ in the presence of 100 μM Rac1 (K_D ~5.33μM; **Figure 2B**, golden vs. purple). Therefore, supplying Rac1 to the D site by covalent tethering has the same effect in promoting Arf1 binding as supplying free Rac1 to a WRC with a blocked A site.

The above assays confirm that Rac1 binding to the D site is essential for enhancing Arf1 binding, but also show mutating or blocking the A site dampens this effect (**Figure 2A**, lane 7; **Figure 2B**, purple). This indicates that Rac1 binding to the A site should also play a role, which might have eluded detection in the assays described above due to the low affinity of the A site for Rac1. The potential cooperativity between A and D sites could further reduce A site binding when the D site is disrupted (Chen et al., 2017; Ding et al., 2022). To examine the contribution of the A site more directly, we stabilized Rac1 binding to the A site by inserting a Rac1 between Y423/S424 in a non-conserved surface loop near the A site (termed ΔWRC230$^{A\text{-}Rac1}$; **Figure 2D**, cartoon). This strategy had allowed us to determine the cryo-EM structure of the WRC with Rac1 bound to the A site and D site simultaneously (Ding et al., 2022). We found that, without free Rac1, tethering Rac1 to the A site mildly promoted Arf1 binding (**Figure 2D**, lane 3 vs. 5). Adding free Rac1 to ΔWRC230$^{A\text{-}Rac1}$ to occupy the D site further enhanced Arf1 binding (**Figure 2D**, lane 6). These data suggest Rac1 binding to the A site partially contributes to Arf1 binding. Taken together, we conclude Rac1 binding to both A and D sites plays a role in promoting Arf1 binding to the WRC, but with the D site having a major contribution as compared to the A site.

279

280 **Arf1 promotes WRC activation using a novel mechanism distinct from Rac1**

281 Arf1 and Rac1 were shown to cooperatively promote WRC activation on lipid-
282 coated beads (Koronakis et al., 2011). Since Rac1 binding to the A site is sufficient to
283 activate the WRC through an allosteric mechanism (Ding et al., 2022), the question
284 remains: does Arf1 binding merely increase the membrane recruitment of WRC, contribute
285 to the same allosteric changes driven by Rac1 binding to the A site, or promote WRC
286 activation through an entirely different mechanism?

287 To distinguish between these possibilities, we first tested if Arf1 differentially binds
288 to the WRC in the autoinhibited ("closed") or activated ("open") state. Previous studies
289 showed that, as an activator, Rac1 had higher affinity for the "open" conformation
290 represented by ΔWRC230 (which lacks the WCA) than for the "closed" conformation
291 represented by the WRC that contained WCA (WRC230WCA; **Figure 3A**, cartoon) (Chen
292 et al., 2017, 2010). If Arf1 is an activator, it should similarly prefer the "open"
293 conformation. Indeed, we observed less binding for WRC230WCA than ΔWRC230, both
294 in the presence and absence of Rac1 (**Figure 3A**). Our EPD assay further confirmed this
295 observation (**Figures 3B** and **S1E**). In the absence of free Rac1, Arf1 had very low binding
296 affinity for WRC230WCA, with a K_D (~107 μM) ~5 times of ΔWRC230 (~22.6 μM)
297 (**Figure 3B**, blue vs. black). Addition of a saturating concentration of Rac1 (100 μM)
298 enhanced Arf1 binding to both WRC230WCA and ΔWRC230, although not to the same
299 level (K_D ~8.2 μM for WRC230WCA vs. K_D ~0.66 μM for ΔWRC230) (**Figure 3B**, purple
300 vs. orange). These data indicate Arf1 distinguishes the "closed" vs. the "open"
301 conformation and therefore may act as an activator of the WRC.

We next measured whether Arf1 could promote WRC activation in the pyrene-actin polymerization assay in aqueous solution (as opposed to on membranes as in the previous study (Koronakis et al., 2011)) (**Figure 3C-E**). For this, the Arf1 construct used in this study does not contain the N-terminal amphipathic helix (also referred to as Arf1$^{\Delta N17}$). This helix is important for Arf1 to bind membranes, but is usually dispensable for binding downstream effectors and therefore often removed in biochemical and structural studies (Dong et al., 2012; Ren et al., 2013). In the absence of Rac1, Arf1 had no obvious effect on WRC activity, potentially due to its low binding affinity to WRC230WCA (**Figure 3C**, brown; **3D**, black). In the presence of low concentrations of Rac1, however, Arf1 enhanced WRC activation in a dose-dependent manner (**Figure 3C**, red curves; **3D**, red, blue). The enhanced WRC activation depended on Arf1 GTP-binding as Arf1 loaded with GDP had no such an effect (**Figure 3C-D**, dashed lines).

The above data suggest that, in addition to potentially recruiting WRC to the plasma membrane, Arf1 directly contributes to WRC activation. Due to the presence of free Rac1 in the above reactions, however, these data cannot tell whether Arf1 acts by promoting the same conformational changes driven by Rac1 binding to the A site, or by directly activating the WRC through a separate mechanism. To distinguish between these two mechanisms, we further tested if Arf1 could activate the WRC230WCA in which a Rac1 molecule was tethered to the D site (WRC$^{\text{D-Rac1}}$; **Figure 3E**, cartoon) (Ding et al., 2022). In this construct, the tethered Rac1 does not activate the WRC (Ding et al., 2022) (also see **Figure 3E**, yellow solid curve), but can promote Arf1 binding to the WRC (**Figure 2C**), allowing us to determine whether Arf1 can activate WRC in the absence of a Rac1 molecule acting through the A site. Remarkably, in the absence of free Rac1, we found Arf1 activated

325 $WRC^{D\text{-}Rac1}$ in a dose-dependent manner (**Figure 3E**, red solid curves), while Arf1 loaded
326 with GDP had no such effect (**Figure 3E**, red dotted curve). To rule out the possibility that
327 Arf1 may activate WRC by mimicking Rac1 binding to the A site, we disrupted the A site
328 by the point mutation C179R and found Arf1 still activated $WRC^{D\text{-}Rac1}$ in a dose-dependent
329 manner (**Figure S3A**), although with reduced potency perhaps because the mutation
330 indirectly weakened Arf1 binding. Together, the above data suggest that Arf1 binding can
331 directly activate WRC, at least *in vitro*, and the Arf1-mediated activation does not involve
332 an interaction of either Rac1 or Arf1 with the A site. Therefore, Arf1 must use a novel
333 mechanism to drive WRC activation.

334 It is important to note that the Arf1-mediated WRC activation reached levels similar
335 to those achieved with Rac1 binding to the A site (**Figure 3E**, black and yellow dotted
336 curves), suggesting Arf1 binding activates the WRC by releasing the WCA, instead of by
337 causing protein aggregation (which is believed to cause artificial WRC activation to a much
338 larger extent than the release of WCA) (Eden et al., 2002; Gautreau et al., 2004; Lebensohn
339 and Kirschner, 2009). This is consistent with our dynamic light scattering (DLS)
340 measurement showing that Arf1 did not promote WRC aggregation (**Figure S2J**).

341

342 **Arf1 binds to a conserved site distinct from Rac1 binding sites**

343 How does Arf1 binding activate WRC? To answer this question, we determined the
344 Arf1 binding site by combining protein docking, surface conservation analysis,
345 mutagenesis, and molecular dynamics simulation (**Figures 4, 5, S4, S5**). We first searched
346 for potential binding sites by using several different protein docking programs, including
347 ClusPro (Desta et al., 2020), HADDOCK (Van Zundert et al., 2016), InterEvDock

(Quignot et al., 2018), FRODOCK (Ramírez-Aportela et al., 2016), and HDOCK (Yan et al., 2020). During the search, we restrained the Switch I and Switch II motifs of Arf1 in close contact with the WRC, since they usually mediate GTPase-effector interactions. Combining the docking results with the surface conservation analysis of the WRC by Consurf (Ashkenazy et al., 2016), we selected a series of conserved surface patches, mutated the solvent-exposed residues individually or in combination, purified the mutant WRCs, and used pull-down assays to examine if any mutations could disrupt Arf1 binding (**Figure S4**).

Out of over 12 conserved surfaces that we surveyed, one surface specifically disrupted Arf1 binding (**Figure S4A**, M1 site; **S4F,** lane 6; **Figure 5A,** lane 10). We named this site the M site since it is in the **m**iddle of the WRC, sandwiched between the D site and the W helix of the WCA (**Figure 4A**). The M site is a small, conserved, and slightly negatively charged surface patch on Sra1 (**Figure S4A, B**). Mutating the conserved surface residues at the M site, either Y986A/E988A (ΔM#1) or Y948A/T951A (ΔM#2), disrupted Arf1 binding, whereas mutating two other conserved residues, W845A/Y849A (ΔM#3), near the M site did not disrupt Arf1 binding (**Figure 4B**; **Figure 5A**, lane 10-12; **Figure S4F**), suggesting the effect of ΔM#1 and ΔM#2 was specific to Arf1 binding. Furthermore, the WRC carrying ΔM#1 or ΔM#2 mutations could not be further activated by Arf1 (**Figures 5B, C** and **S3B**). It's important to note that the M site mutations only disrupted Arf1-mediated activation, but not Rac1-mediated activation (**Figures 5D** and **S3B**). Thus, these surface mutations are specific in disrupting Arf1 binding and Arf1-mediated activation, without affecting WRC folding (**Figure S2C-G**) or disturbing Rac1-mediated activation.

Note all four residues are highly conserved in animals (**Figure 4E**). In particular, Y986 remains strictly Tyrosine from human to sponge, while E988 is only exchangeable with Aspartate. In non-animal species they are either partially conserved (such as in amoeba) or not conserved (such as in plants) (**Figure 4E**). This suggests the Arf-WRC interaction is important for processes unique to animals.

To further define the binding mechanism, we applied molecular dynamics (MD) simulation to optimize binding poses of the top 6 docking models that placed Arf1 at the M site (**Figure S5A, B**). We then evaluated different models by calculating the molecular mechanics/Poisson–Boltzmann surface area/weighted solvent accessible surface area (MM-PBSA-WSAS) free energies of the whole complex and the binding free energy between Arf1 and WRC (**Figure S5C-I**). Out of the 6 docking models, model C8 gave the lowest binding free energy (**Figure S5G, I**). Importantly, introducing ΔM#1 or ΔM#2 mutations onto model C8 increased the binding energy, suggesting they destabilized Arf1-WRC interaction. By contrast, introducing the control mutation ΔM#3 did not affect the binding energy (**Figure S5I**). These data are consistent with our pull-down assays showing only ΔM#1 & 2, but not ΔM#3, disrupted Arf1 binding (**Figure 5A, S4F**).

Note that it was previously shown the M371V mutation in Hem1 (M373V in Nap1) found in human patients interfered with (but did not abolish) Arf1 binding and WRC activation (Cook et al., 2020). The above analysis suggests M371 is not the Arf1 binding site. Rather, the effect of M371V was likely indirect, as this residue is located at the bottom of a deep pocket neighboring the D site, where it was difficult to accommodate an Arf1 molecule (**Figure S4A**).

The MD-optimized model sheds light on how Arf1 binds and activates WRC. First, the interaction is mediated by the Switch I motif (**Figures 4C** and **S5G**), the same region that binds to EspG (Dong et al., 2012), explaining how EspG competes off WRC binding to inhibit phagocytosis during pathogenic *E. coli* infection (Humphreys et al., 2016) (**Figure 1B**). Second, the interaction mainly involves hydrogen bonding between Y986 and E988 in Sra1 and T44 and T45 in Arf1, with Y948 or T951 in Sra1 contacting I46 and T44 in Rac1 through Van der Waals interactions (**Figures 4C** and **S5G**). This explains why Y986A/E988A (ΔM#1) disrupted Arf1 binding more severely than Y948A/T951A (ΔM#2) in GST pull-down assays (**Figures 5A** and **S4F**), and is also consistent with our observation that Arf1 binding is sensitive to pH and salt concentration (**Figure 1E**). Third, the relative orientation of Arf1 is compatible with the model of how WRC is oriented on the membrane together with two Rac1 molecules (**Figure 4D**) (Chen et al., 2017, 2010; Ding et al., 2022). In this orientation, the N-terminus of $Arf1^{\Delta 17}$ is near the plasma membrane (**Figure 4D**, arrow), which would allow its N-terminal amphipathic helix to associate with membranes. Finally, this model explains how Arf1 binding may activate the WRC. Arf1 is located near (but not in direct contact with) the W helix of WCA (**Figure 4D**). Therefore, distinct from Rac1-mediated WRC activation, which involves a series of conformational changes propagating from the A site to a conserved region around $WAVE1^{Y151}$ (referred to as Tyrosine lock) to release the WCA (Ding et al., 2022), Arf1 binding may contribute to WRC activation by directly perturbing the W helix located in its proximity (see models in **Figure 7**).

The identification of the M site allowed us to specifically probe the function of the Arf1-WRC interaction in the cell. WRC is key to actin polymerization at plasma

membranes and formation of sheet-like protrusions known as lamellipodia and membrane ruffles commonly found at the leading edge of migrating or spreading cells (Rottner et al., 2021; Takenawa and Suetsugu, 2007) (**Figure 6A**). In our previous complementation assays using B16-F1 cells genetically disrupted for both *Sra1* and *Cyfip2* genes, mutating the A site almost completely abolished WRC-mediated lamellipodia formation, while mutating the D site impaired (but did not eliminate) actin assembly and lamellipodia morphology (Schaks et al., 2018, 2020). Using the same assay, we found mutating the M site produced phenotypes nearly identical to mutating the D site (**Figure 6B-D**). In both cases, mutations led to narrow actin networks and reduced the formation frequency of mature lamellipodia, but without affecting WRC localization or assembly (**Figure 6B, D)**. Interestingly, when we combined the M site and D site mutations into one construct, they did not aggravate the phenotype, except that the ΔD/ΔM#2 dual mutations slightly decreased the total percentage of lamellipodia-containing cells (**Figure 6E-G**). Together, the above results suggest that the M and D sites act in the same mechanistic pathway to regulate lamellipodial morphology, with Arf1 binding to the M site likely acting downstream of Rac1 binding to the D site (see *in vitro* data above).

Discussion

By biochemical reconstitution and structural analysis, our work establishes that Arf1 directly interacts with the WRC through a previously unidentified conserved surface located on Sra1. We show that, although intrinsically weak, this interaction can be greatly enhanced by Rac1 binding to the D site. Once bound to the WRC, Arf1 can independently drive WRC activation, at least *in vitro*, by using a mechanism distinct from that mediated

by Rac1 binding to the A site. We further demonstrate that disrupting Arf1-WRC interaction by point mutations specifically abolishes Arf1-mediated (but not Rac1-mediated) WRC activation, and impairs WRC-mediated lamellipodia formation. Our work has important implications on the regulation of the actin cytoskeleton in many different biological systems.

First, our study established a new mechanism underlying WRC activation. The WRC is a central signaling hub through which a large diversity of membrane ligands can transmit signals to Arp2/3 complex-mediated actin polymerization (Chen et al., 2014b, 2017; Lebensohn and Kirschner, 2009; Rottner et al., 2021). Despite the long list of WRC ligands, Rac1 has been known as the only activator that is both necessary and sufficient—at least *in vitro*—to activate WRC (Chen et al., 2017; Schaks et al., 2018). While other ligands may act cooperatively with Rac1 to further tune WRC activity, exactly how they do so is completely unknown (Chen et al., 2014b, 2014c; Koronakis et al., 2011; Lebensohn and Kirschner, 2009). In particular, how Arf1 facilitates WRC activation has remained enigmatic for many years. It was not known if Arf1 can directly interact with WRC, and if yes, how Arf works together with Rac1 to promote WRC activity (Singh et al., 2019). Our work provides firm answers to these questions, revealing that significant Arf1 binding relies on Rac1 binding mainly to the D site, but Arf1 binding can directly promote WRC activity even independently of Rac1 binding the A site. These results establish Arf1 as a second, genuine activator of the WRC and provides a mechanism to explain the cooperativity between Arf1 and Rac1 previously observed both *in vitro* and in cells (Boshans et al., 2000; Koronakis et al., 2011; Radhakrishna et al., 1999; Santy and Casanova, 2001).

Second, our study lays a foundation for studying how WRC-mediated actin polymerization connects various Arf- and Rac1-mediated processes. Our work identifies point mutations that can specifically disrupt Arf binding and Arf-mediated (but not Rac1-mediated) WRC activation. These mutations will be powerful tools for dissecting the role of the Arf-WRC-Arp2/3-actin signaling axis from the canonical Rac1-WRC-Arp2/3-actin axis. Arf-family GTPases play an important role in various membrane trafficking processes, with some of them tightly connected to actin cytoskeleton regulation (Myers and Casanova, 2008; Singh et al., 2017; Sztul et al., 2019). On the other hand, new roles of actin, WRC, and Arp2/3 complex are emerging, suggesting their importance in the endomembrane systems beyond their canonical role in driving plasma membrane protrusions (Anitei et al., 2010; Cheng et al., 2007; Kang et al., 2010; Sung et al., 2008). We thus posit that Arf-mediated WRC activation provides the cell with an additional pathway for promoting WRC activation and actin polymerization, the precise outcome of which will likely depend on relative local membrane densities of Rac1 vs. Arf (**Figure 7**). Specifically, Rac1 binding to the high-affinity D site may serve as a general recruitment mechanism to prime the WRC on the membrane without causing activation. Then, depending on specific upstream signals in distinct cell types and tissues leading to activation of various Arf- or Rac1-GEFs, the precise tuning of WRC activation in given condition and system will depend on the local density of activated Rac1 or Arf molecules, which can subsequently trigger WRC activation by distinct structural mechanisms (**Figure 7**).

Third, the Arf binding site is highly conserved in animals, from human to sponge, but is only partially conserved in other organisms and is not conserved in plants. This suggests that the function of Arf1-mediated WRC activation is likely important for

processes unique to animals, such as neuronal outgrowth and synapse formation, immune cell chemotaxis and activation, and cancer cell migration and metastasis, in all of which Arf and WRC play important roles (Donaldson and Jackson, 2011; Myers and Casanova, 2008; Rottner et al., 2021; Singh et al., 2017; Sztul et al., 2019). In non-animal species, while sequence analysis of the M site suggests the direct interaction between Arf and the WRC is perhaps lost (**Figure 4E**), considering the conserved importance of Arf and WRC in non-animal species, we cannot rule out the possibility that the M site surface and Arf molecules may still have co-evolved to keep the connection between Arf and the WRC maintained. Our work raises the possibility of exploring the role of Arf-related processes in WRC-mediated actin polymerization in both animal and non-animal organisms.

Together, this work uncovers a new, conserved mechanism underlying WRC activation, and provides a foundation for exploring the regulation of the actin cytoskeleton in multiple processes in which Rac and the various Arf-family GTPases may intimately cooperate.

Acknowledgements

We thank Shae Padrick at Drexel University for updating the published python codes for actin data analysis, Aubrey Sijo-Gonzales, Finlan Rhodes, Leyuan Loh, Ganesh Prasad, Simanta Mitra, and the ResearchIT at Iowa State University for migrating the python codes to the web-based application, Scott Nelson at Iowa State for use of the fluorimeter, Daniel Rosenbaum at UT Southwestern for providing the PGS construct, and Neal Alto at UT Southwestern for providing various Arf, Arl, and EspG constructs. Research was supported by funding from the National Institutes of Health (R35-GM128786) and Iowa State

University and Roy J. Carver Charitable Trust start-up funds to B.C., Stony Brook University start-up funds to S.C., the Deutsche Forschungsgemeinschaft (DFG), Research Training Group GRK2223, and individual grant RO2414/8-1 to K.R, the National Institutes of Health (R01-DK107733) to D.D.B., and the National Science Foundation (1955260) and National Institutes of Health (R01-GM079383) to J.W.

Author contributions

B.C. conceived the project and oversaw biochemical work. K.R. oversaw cell biological work. J.W. performed MD simulation and energy calculation. S.Y. purified proteins and performed biochemical experiments. Y.L. and A.B. helped with protein purification and biochemical assays. M.S. performed cellular experiments. B.D. and S.C. helped with structural analysis. D.A.K. performed DLS analysis. L.D., O.A., and D.D.B. helped with cell biological analysis. B.C. wrote the manuscript and prepared figures with assistance from all authors.

Declaration of interests

The authors declare no competing interests.

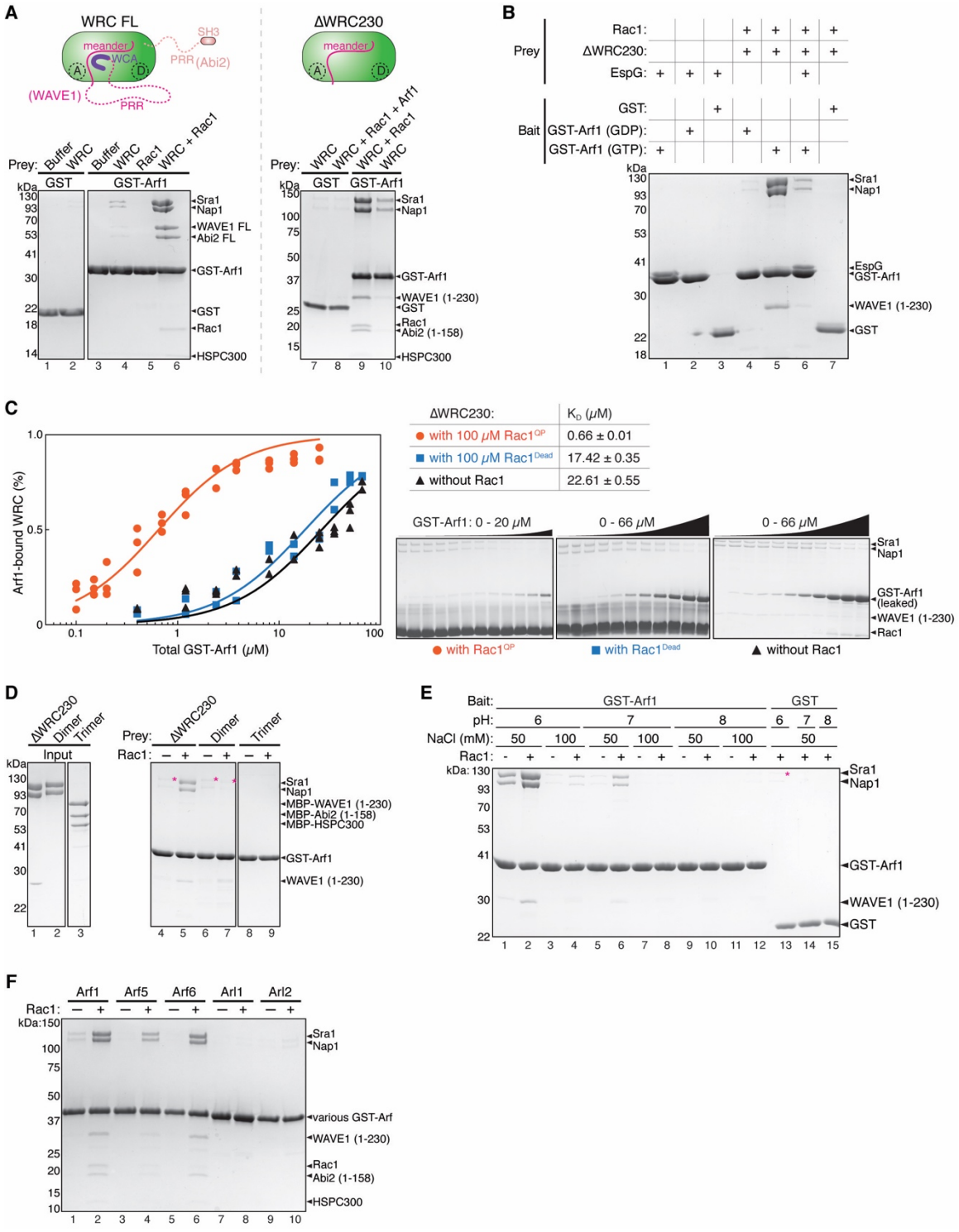

Figure 1. Arf-WRC interaction is direct and can be greatly enhanced by Rac1. (A) Coomassie blue-stained SDS-PAGE gels showing GST-Arf1 pull-down of WRC FL (left) and ΔWRC230 (right) in the presence or absence of untagged Rac1^{QP}. In the schematic of

respective WRCs, dotted lines indicate unstructured sequences. Both the A and D sites for Rac1 binding are indicated. **(B)** Coomassie blue-stained SDS-PAGE gels showing pull-down of ΔWRC230 by GST-Arf1 in indicated nucleotide states or in the presence of the Arf1-binding protein EspG. **(C)** Equilibrium pull-down (EPD) assay to measure the binding affinity of the Arf1-WRC interaction in the presence of indicated Rac1 variants. On the left is the quantification of the data pooled from two to three independent experiments for each condition and globally fitted to obtain the binding isotherms. The derived dissociation constant (K_D) and fitting errors are shown in the table. On the right are representative Coomassie blue-stained SDS-PAGE gels of the supernatant samples use for quantification. **(D)** Coomassie blue-stained SDS-PAGE gels showing GST-Arf1 pull-down of WRC subcomplexes in the presence or absence of $Rac1^{QP}$. Dimer is the Sra1/Nap1 subcomplex. Trimer is the WAVE1 (1-230)/Abi2(1-158)/HSPC300 subcomplex. Asterisks indicate weak binding signals. **(E)** Arf1 binding to the WRC is sensitive to pH and salt concentration. Shown is Coomassie blue-stained SDS PAGE from GST-Arf1 pull down of ΔWRC230 in indicated buffer conditions, in the presence or absence of $Rac1^{QP}$. Red asterisk indicates increased background binding to GST beads at pH 6, to avoid which we use pH 7 and 50 mM NaCl throughout this study. **(F)** Coomassie blue-stained SDS-PAGE gel showing pull-down of ΔWRC230 by different GST-tagged Arf-family members with or without $Rac1^{QP}$.

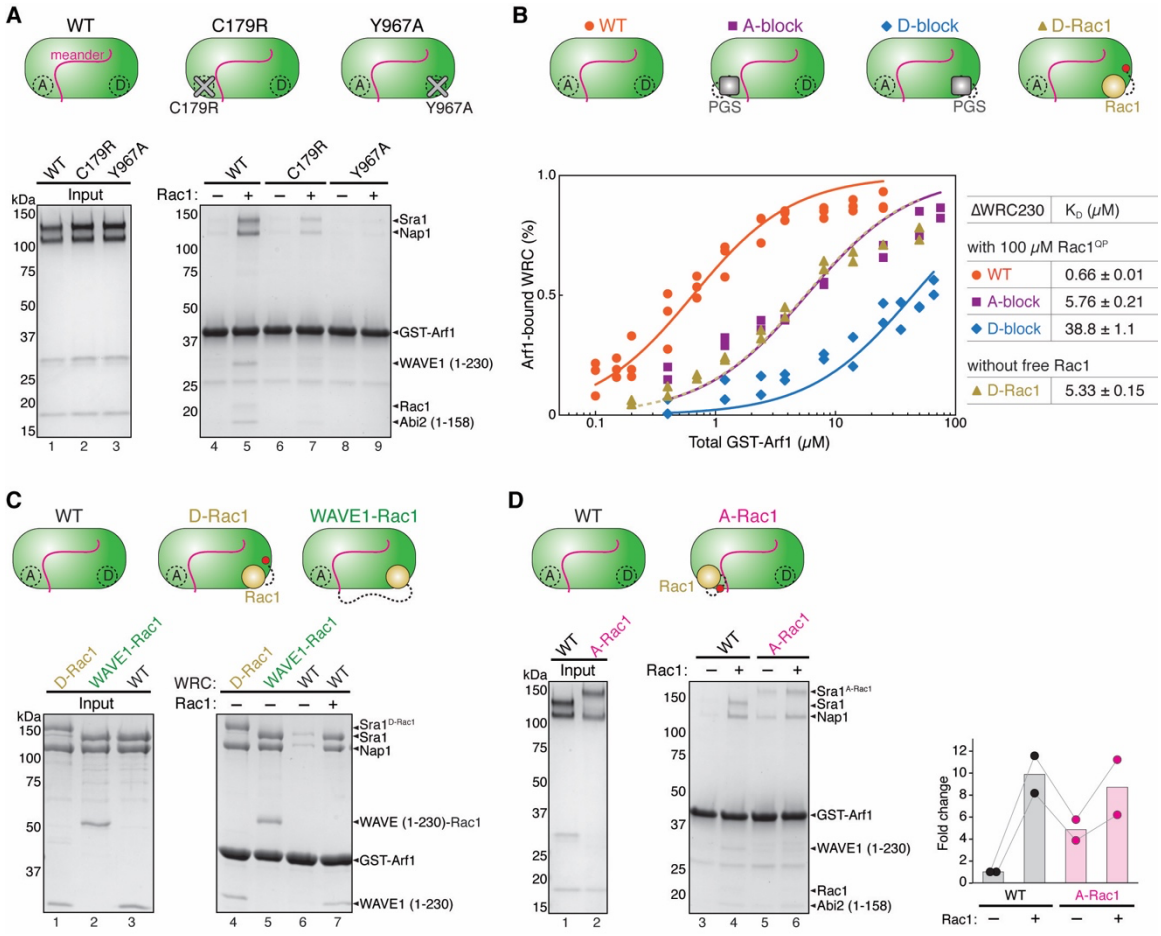

552

553 **Figure 2. Arf1 binding mainly depends on Rac1 binding to the D site. (A)** Coomassie
554 blue-stained SDS-PAGE gels showing GST-Arf1 pull-down of WRC bearing point
555 mutations in Sra1 that specifically disrupt the A or D site. **(B)** EPD assay measuring the
556 binding affinity of GST-Arf1 for the indicated ΔWRC230 constructs in the presence or
557 absence of 100 μM Rac1^{QP}. Data for each mutant are pooled from two independent
558 experiments. Data for the WT WRC are taken from Figure 1C and used here as a reference
559 point. See Figure S1 for representative gel images. **(C)** Coomassie blue-stained SDS-PAGE
560 gels showing GST-Arf1 pull-downs of WRCs with Rac1 tethered to indicated positions to
561 stabilize Rac1 binding to the D site. **(D)** Coomassie blue-stained SDS-PAGE gels showing
562 GST-Arf1 pull-down of WRCs with Rac1 inserted between Y423/S424 of the surface loop

(a.a. 418-432) to stabilize Rac1 binding to the A site. Shown on the right is the gel quantification of the Sra1-Nap1 bands normalized to GST-Arf1 bands from two independent repeats, with the data from each repeat connected. In the schematic of WRCs, red dots indicate the tethering points of Rac1 to A or D site.

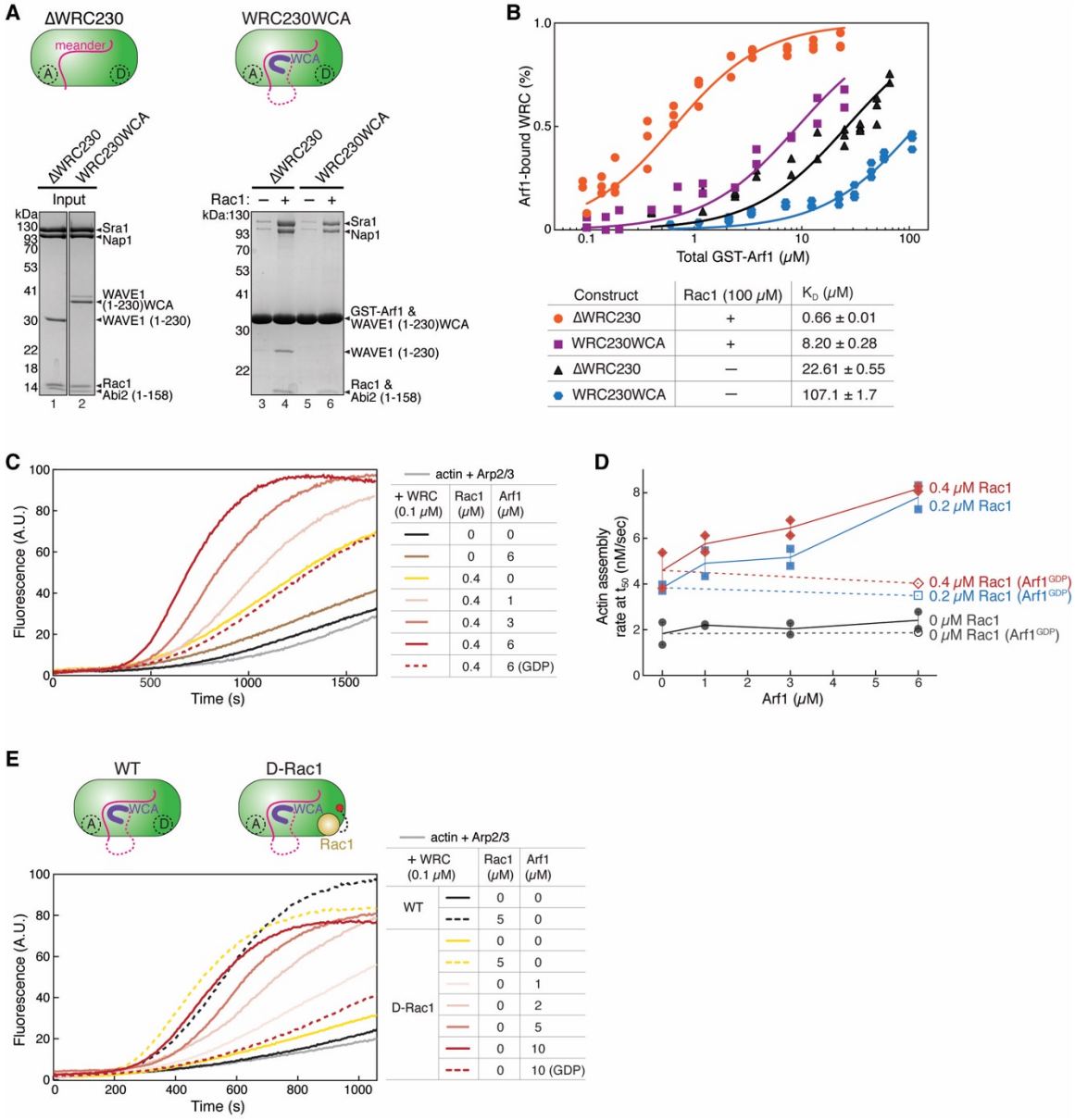

568

569 **Figure 3. Arf1 promotes WRC activation independent of Rac1 binding to the A site.**

570 **(A)** Coomassie blue-stained SDS-PAGE gels showing GST-Arf1 pull-down of WRC with

571 or without the WCA sequence. **(B)** EPD assay comparing the binding affinity of GST-Arf1

572 for the WRC with or without the WCA sequence. Data for WRC230WCA are pooled from

573 two independent experiments for each condition. Data for the ΔWRC230 are taken from

574 Figure 1C and used here as a reference point. See Figure S1 for representative gel images.

575 **(C-D)** Representative pyrene-actin polymerization assay (C) and quantification of the actin

polymerization rate at t_{50} (D) (Doolittle et al., 2013) measuring activity of WRC230WCA in the presence of indicated concentrations of $Rac1^{QP}$ and Arf1. **(E)** Pyrene-actin polymerization assay of the WT WRC230WCA vs. $WRC^{D\text{-}Rac1}$ in response to the addition of free $Rac1^{QP}$ or Arf1. Reactions in (C-E) contain 3.5 μM actin (5% pyrene labeled), 10 nM Arp2/3 complex, 100 nM WRC, and indicated amounts of Rac1 and/or Arf1. In all assays, Arf1 is loaded with GMPPNP, unless it is indicated with GDP.

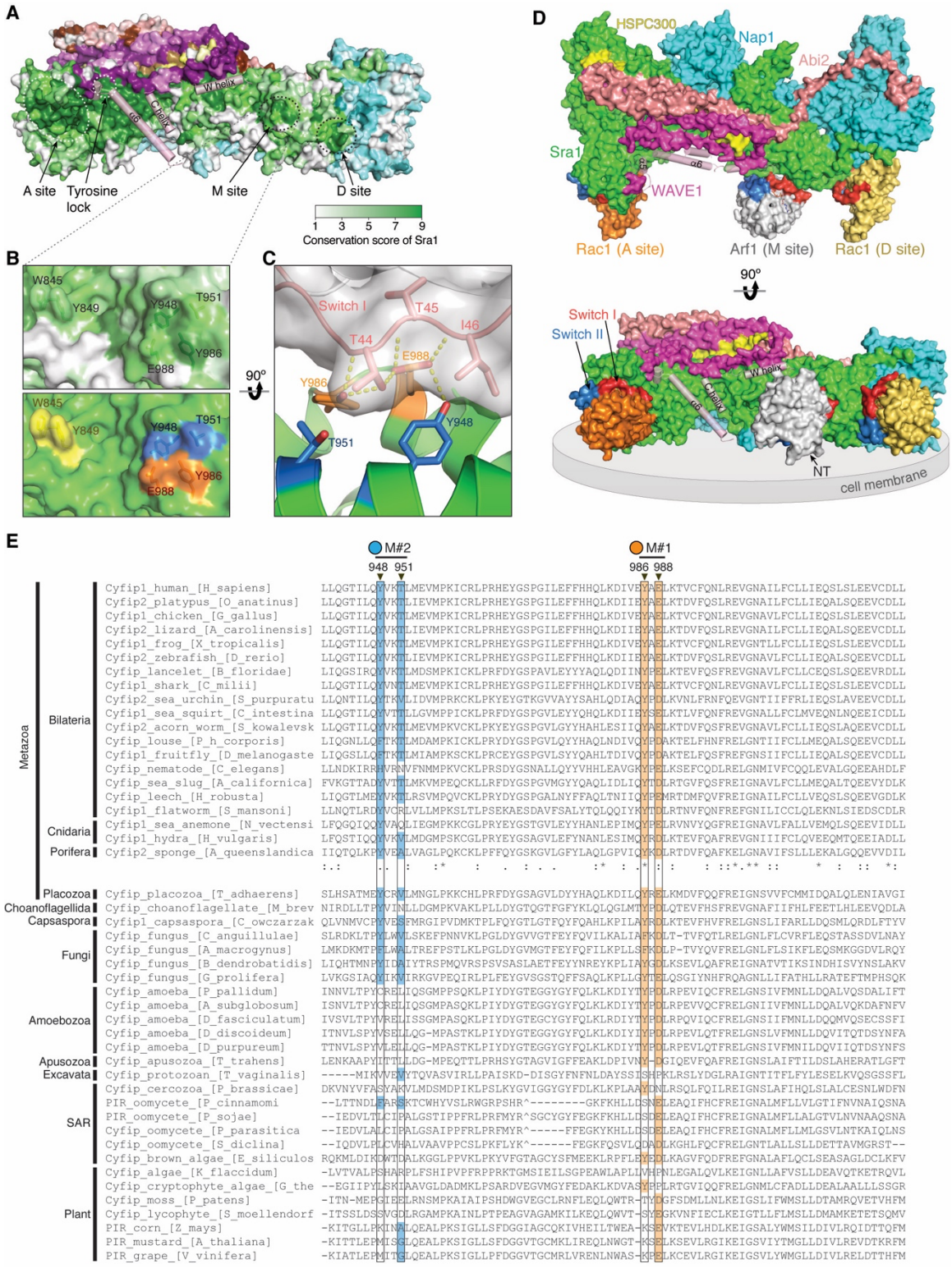

583

584 **Figure 4. Arf1 binds to a conserved site distinct from Rac1 binding sites. (A)** Surface

585 conservation of the WRC, with color to white gradients representing the most conserved

surface residues (ConSurf score = 9 for darkest colors) to the least conserved residues (ConSurf score = 1 for white color) (Ashkenazy et al., 2016). Important sites on Sra1, including the identified Arf1 binding site (M site), are indicated with dotted circles. Semitransparent pink cylinders refer to the sequence in WAVE1 that are destabilized upon WRC activation by Rac1 (Ding et al., 2022). **(B)** Close-up view of the M site showing surface conservation (top) and surface patches to be mutated (bottom, colored using the same scheme in Figure 5A). **(C)** Side view showing the interaction between Arf1 and the M site in the MD-optimized model C8. Contacting residues are shown as sticks. Yellow dotted lines indicate polar interactions. **(D)** Surface representation of the overall structural model of the WRC bound to two Rac1 molecules (PDB: 7USE) (Ding et al., 2022) and one Arf1 molecule (PDB: 1J2J). Position of Arf1 shows the MD-optimized docking solution C8, which has the lowest binding free energy. Switch I and II elements of Rac1 and Arf1 GTPases are red and blue, respectively. Grey disc demonstrates the predicted orientation of the WRC at the inner surface of the plasma membrane. The N-terminus of Arf1$^{\Delta N17}$ used in this study is indicated with arrow. **(E)** Sequence alignments of Sra1 from representative eukaryotic organisms. Surface residues of the M site (black boxes) are highlighted with orange for the M#1 surface patch and blue for M#2, as indicated by black arrowheads on top. Degrees of conservation in animals (up to Porifera) are represented with ClustalW symbols (Thompson et al., 1994)(* for no change, : for conserved, . for less conserved changes). '-' for missing amino acids; '^' for amino acid insertions in alignments that were not shown.

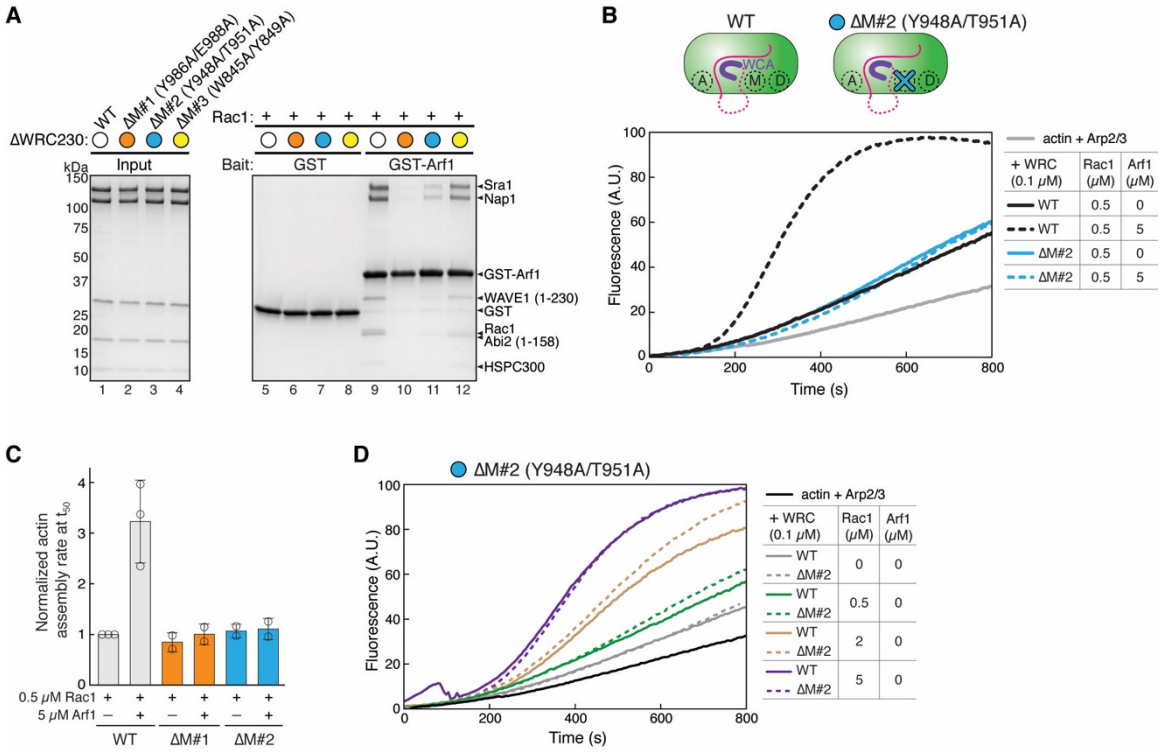

Figure 5. M site mutations disrupt Arf1 binding and Arf1-mediated WRC activation. **(A)** Coomassie blue-stained SDS-PAGE gels showing GST pull-down of ΔWRC230 bearing the indicated mutations in Sra1 at the M site. **(B-C)** Representative pyrene-actin polymerization assay (B) and quantification of the actin polymerization rate at t_{50} normalized to WT WRC230WCA + 0.5 μM Rac1 (C), measuring the effect of M site mutations on WRC activation by Arf1. Reactions contain 3.5 μM actin (5% pyrene labeled), 10 nM Arp2/3 complex, 100 nM WRC230WCA (WT or indicated mutants), and indicated amounts of $Rac1^{QP}$ and/or Arf1 loaded with GMPPNP. Error bars represent standard errors of means. **(D)** Comparison of the WT WRC to the ΔM#2 (Y948A/T951A) mutant activated by different amounts of $Rac1^{QP}$. Reactions were performed in the same conditions as in (B).

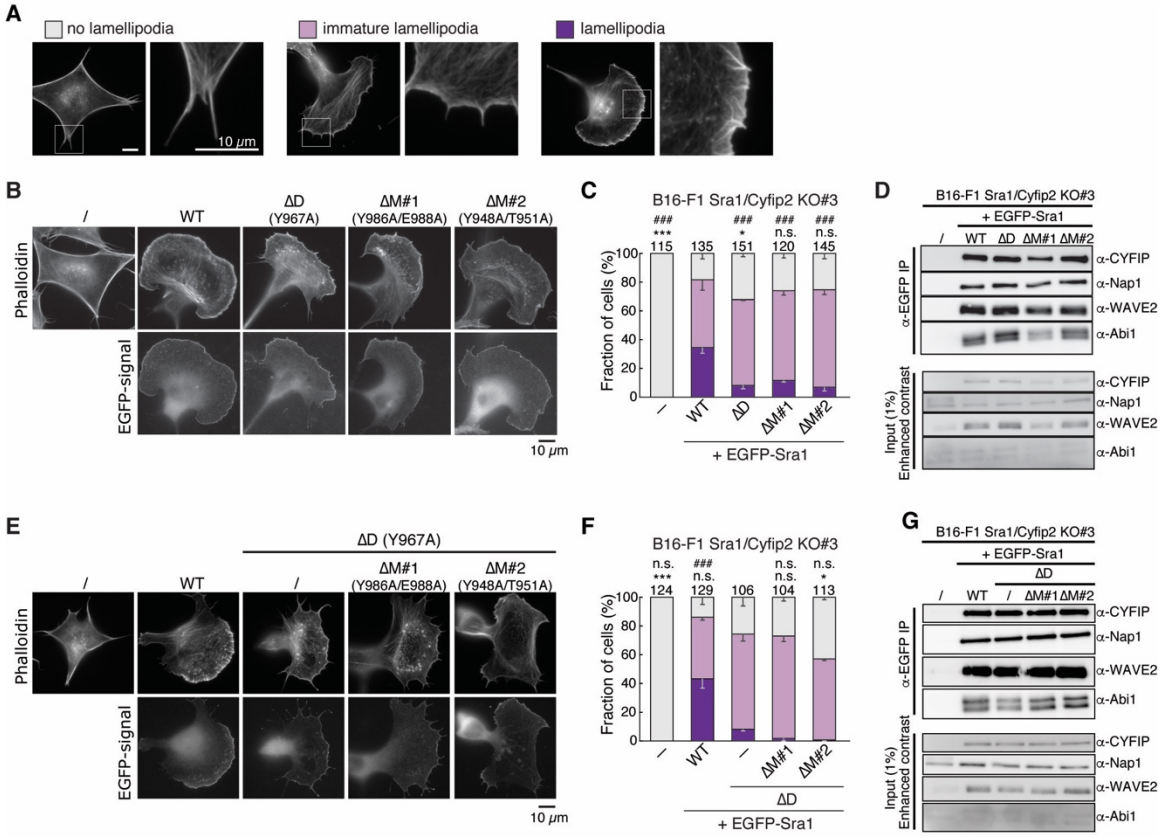

620

621 **Figure 6. M site mutations impaired lamellipodia morphology. (A, B, E)**
622 Representative fluorescence images of lamellipodia formation in B16-F1 *Sra1/Cyfip2*
623 double KO#3 cells transfected with indicated EGFP-Sra1 variants and stained by phalloidin
624 for F-actin. Images show representative examples of the cell morphologies used for
625 categorization of induced effects below. ΔD for Sra1^{Y967A}, which disrupts the D site. ΔM
626 #1 for Sra1$^{Y986A/E988A}$. ΔM #2 for Sra1$^{Y948A/T951A}$. **(C, F)** Quantification of lamellipodial
627 morphologies. Statistical significance was assessed from 3 repeats for differences between
628 cells transfected with WT (wild type) (**C**) or ΔD (**F**) vs. no (-) or indicated constructs
629 concerning cell percentages displaying "no lamellipodia" phenotype (* $p < 0.05$; *** $p <$
630 0.001) and with "lamellipodia" phenotype (### $p < 0.001$). n.s.: not statistically significant.
631 Error bars represent standard errors of means. Numbers of cells used in the quantification
632 are shown on top of each column. **(D, G)** Immunoprecipitation (IP) and Western blot of

633 the same B16-F1 *Sra1/CYFIP2* double KO#3 cells used in (B & C and E & F), respectively.
634 The cells were transfected with indicated EGFP-tagged Sra1 variants, lysed, and probed
635 for the expression and assembly of WRC, as exemplified by CYFIP (for both Sra1 and
636 Cyfip2), Nap1, WAVE2, and Abi1.
637

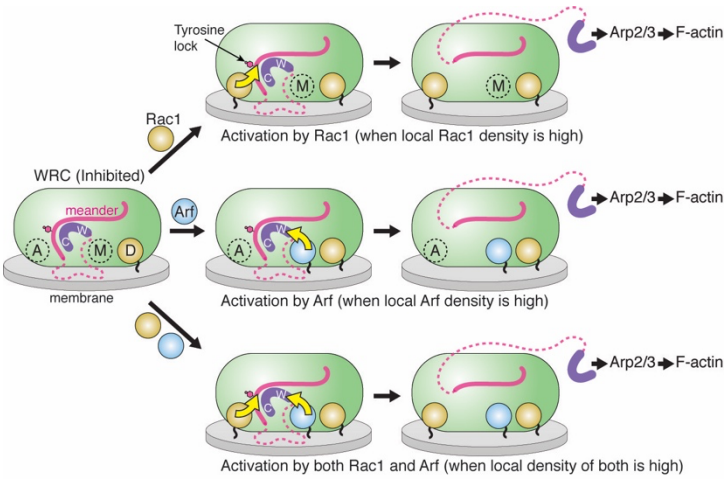

Figure 7. Rac1 and Arf may act both cooperatively and separately to promote WRC activation. Schematic showing how the WRC can be activated by Rac1 (top), Arf (middle) and both (bottom) through specific mechanisms that can arise independently from each other. Structural elements critical to WRC inhibition and activation are shown. Yellow arrows indicate structural pathways leading to WRC activation. Magenta dashed lines represent unstructured sequences in WAVE1. Black wiggly lines attached to Arf and Rac1 represent membrane binding sequences and lipid modifications of the GTPases. Rac1 first engages with the D site due to its relatively high affinity, which primes the WRC on the membrane without causing activation (left). When Rac1 density on the membrane is high (top), further binding of Rac1 to the A site promotes WRC activation by allosterically destabilizing the Tyrosine lock region, which subsequently releases Y151 (indicated by pink hexagon) and the WCA (purple) (Ding et al., 2022). Alternatively, when Arf1 density on the membrane is high (middle), Rac1 at the D site promotes Arf binding to the M site, which in turn, through its close proximity to the W helix, can perturb WCA binding to promote WRC activation. The remaining part of the schematic displays the functional

654 outcome of both mechanisms operating in cooperation to ensure an optimized output

655 response (bottom).

656
657

Methods

Protein purification

All WRC constructs used in this work were derived from previously published WRC230WCA (also called WRC230VCA or WRC^{apo}) and ΔWRC230 by standard molecular biology procedures and were verified by Sanger sequencing (Chen et al., 2014a, 2017; Ding et al., 2022). WRC230WCA contains human full-length Sra1, full-length Nap1, WAVE1(1-230)-$(GGS)_6$-WCA(485-559), Abi2(1-158), and full-length HSPC300. ΔWRC230 also contains the same subunits except that WAVE1(1-230)-$(GGS)_6$-WCA(485-559) is replaced by WAVE1(1-230). Other WRCs contain modified subunits described in detail in **Tables S1** and **S2**.

The WRCs were expressed and purified essentially as previously described (Chen et al., 2014a, 2017). Reconstitution of the recombinant WRC is a multi-step process, involving purification of individual proteins from different host cells (prokaryotic cell and insect cell), assembly/purification of sub-complexes (Sra1/Nap1 dimer and WAVE1/Abi2/HSPC300 trimer) and finally of the WRC pentamer by a series of affinity, ion exchange and gel filtration chromatography steps. Mutations introduced into WRC subunits were carefully chosen and typically made to surface-exposed residues, producing complexes that behaved well and identically to the WT WRC during each step of reconstitution (**Figure S2**). Except Sra1 and Nap1, which were expressed in *Tni* cells using the ESF 921 medium (Expression Systems), other proteins were typically expressed in BL21 $(DE3)^{T1R}$ cells (Sigma) at 18 °C overnight or ArcticExpress^{TM} (DE3) RIL cells (Stratagene) at 10°C for 24 hours. GST-Rac1^{QP} and GST-Rac1^{Dead} were purified by Glutathione Sepharose beads (Cytiva), followed by cation-exchange chromatography

through a Source SP15 column and gel filtration through a Hiload Superdex 75 column. GST-Arf1 was purified by Glutathione Sepharose beads, followed by anion-exchange chromatography through a Source Q15 column and gel filtration through a Hiload Superdex 75 column. His8-$(GGS)_2$-Arf1 and His6-Tev-EspG were purified by Ni-NTA agarose beads (Qiagen), followed by anion-exchange chromatography through a Source Q15 column and gel filtration through a Hiload Superdex 75 column. Untagged $Rac1^{QP}$ and untagged $Rac1^{Dead}$ were purified by SP Sepharose® Fast Flow beads, followed by a Source SP15 column and a Hiload Superdex 75 gel filtration column. Proteins including Arp2/3 complex, actin, WAVE1 WCA, and TEV protease were purified as previously described (Chen et al., 2014a, 2017; Ismail et al., 2009). All ion exchange and gel filtration chromatography steps were performed using columns from Cytiva on an ÄKTA™ pure protein purification system.

Non-equilibrium pull-down assay

Non-equilibrium GST pull-down experiments were performed as previously described (Chen et al., 2017). Typically, 100-200 pmol of GST-tagged proteins as baits and 100-200 pmol of WRCs as preys were mixed with 20 µL of Glutathione Sepharose beads (Cytiva) in 1 mL of binding buffer (10 mM HEPES pH 7, 50 mM NaCl, 5% (w/v) glycerol, 0.05% (w/v) Triton X100, 2 mM $MgCl_2$, and 5 mM β-mercaptoethanol or 1 mM DTT) at 4 °C for 30 min, followed by three washes using 1 mL of the binding buffer in each time of wash. Bound proteins were eluted with the GST elution buffer (100 mM Tris-HCl pH 8.5, 2 mM $MgCl_2$, and 30 mM reduced glutathione) and examined by SDS-PAGE.

Equilibrium pull-down (EPD) assay

Equilibrium pull-down (EPD) experiments were performed essentially as previously described (Chen et al., 2017). Glutathione Sepharose beads (Cytiva) were first equilibrated in EPD buffer (10 mM HEPES pH 7, 50 mM NaCl, 5% (w/v) glycerol, 2 mM $MgCl_2$, and 1 mM DTT) and stored as a 50% (v/v) slurry. Before use, all protein samples were dialyzed against EPD buffer overnight at 4 °C or purified by gel filtration through a column equilibrated with the EPD buffer to maximize buffer match. Each reaction was assembled in 100 µL of total volume of EPD buffer in a 200-µL PCR tube (Axygen), which contained 0.1 µM prey (e.g., WRC), varying concentrations of bait (e.g., GST-Arf1), with or without 100 µM untagged $Rac1^{QP}$ or $Rac1^{Dead}$, 30 µL of the Glutathione Sepharose beads (by aliquoting 60 µL of the 50% (v/v) slurry using a wide-bore pipette tip), and 0.05% (w/v) Triton X100 to facilitate mixing. The reactions were gently mixed at 4 °C on a rotary mixer for 30 min. After a brief centrifugation (~10,000 g for 10 s) to pellet the beads, 40 µL of the supernatant was immediately transferred to 8 µL of 6 X loading buffer (360 mM Tris-HCl pH 6.8, 12% (w/v) SDS, 60% (w/v) glycerol, 0.012% (w/v) bromophenol blue, and 140 mM freshly added β-mercaptoethanol), and analyzed by Coomassie blue-stained SDS-PAGE gels. The gels were imaged by a ChemiDoc™ XRS + system (BioRAD). Total intensity of the Sra1 and Nap1 bands was quantified by ImageJ (FIJI) to determine unbound WRC. The derived fractional occupancy from 2 to 3 independent experiments was pooled to obtain the binding isotherms for global fitting. The program Prism 8 (GraphPad) was used to fit the binding isotherms using the equation below to obtain dissociation constants K_D: $y = \frac{(W+x+K_D)-\sqrt{(W+x+K_D)^2-4*W*x}}{2*W}$, where y is the fractional occupancy, W is the total WRC concentration (typically 0.1 µM), and x is the total GST-Arf1 concentration.

Pyrene-actin polymerization assay

Actin polymerization assays were performed as previously described with some modifications here (Chen et al., 2017). Each reaction (120 µL) contained 3-4 µM actin (5% pyrene labeled), 10 nM Arp2/3 complex, 100 nM of various WRC230WCA constructs or WAVE1 WCA, and desired concentrations of untagged $Rac1^{QP}$ and /or His8-Arf1 in the NMEH20GD buffer (50 mM NaCl, 1 mM $MgCl_2$, 1 mM EGTA, 10 mM HEPES pH7.0, 20% (w/v) glycerol, and 1 mM DTT). We found that compared to the commonly used KMEI20GD buffer (50 mM KCl, 1 mM $MgCl_2$, 1 mM EGTA, 10 mM Imidazole pH7.0, 20% (w/v) glycerol, and 1 mM DTT), the NMEH20GD buffer increased the sensitivity of WRC to Rac1 and Arf1, allowing us to use lower protein concentrations and reduce reaction time in actin assembly assays. Pyrene-actin fluorescence was recorded every 5 seconds at 22 °C, one reaction per measurement using a single-channel pipette to minimize air bubbles or pipetting errors, using a 96-well flat-bottom black plate (Greiner Bio-One™) in a Spark plate reader (Tecan), with excitation at 365 nm and emission at 407 nm (15 nm bandwidth for both wavelengths). Actin assembly rates at the time where the fluorescence intensity is half of the maximum plateau (t_{50}) were derived from the kinetic curves using previously published python scripts (Doolittle et al., 2013), which is also implemented on a web application of the scripts (*https://biochempy.bb.iastate.edu*).

Dynamic light scattering (DLS) measurement

All experiments were performed on a Wyatt DynaPro NanoStar instrument using Dynamics 7.1.7 software. Sample definitions were as follows: Mw-R model: Globular Proteins; dn/dC (mL/g): 0.185; RG Model: Sphere; Cuvette: Glass Cuvette; Solvent Name, Glycerol 5%. Otherwise, default parameters from the instruments were used, including refractive index and viscosity. Proteins and buffers were filtered using 0.22-µm centrifugal

749 filters right before use to ensure dust was removed from samples. Proteins were mixed
750 directly, and 10 μL were loaded into a quartz microcuvette. Each protein mixture was
751 repeated multiple times, with each repeat undertaking 20 acquisitions (5 seconds per
752 acquisition). The cuvette was cleaned by washing three times with filtered MilliQ water,
753 three times with filtered 95% ethanol, then dried using filtered air. Cutoffs for acceptable
754 runs were defined as any run with SOS (sum of squares) less than 10.0 and with a baseline
755 reading between 0.995 and 1.005. Acquisitions exceeding these values were excluded. For
756 each protein mixture, the readings of all acquisitions from multiple repeats were pooled to
757 obtain the average molecule radius and compared for statistical significance of differences
758 using the ANOVA test in the software R.

759 ***Molecular dynamics simulations***

760 We applied molecular dynamics (MD) simulations and free energies to optimize
761 Arf1 and WRC binding poses. In total, we simulated 6 binding poses that placed the Arf1
762 close to the D site. Each MD system consists of one WRC bound to two Rac1 molecules
763 (PDB: 7USE) (Ding et al., 2022), one Arf1 (PDB: 1J2J), 400 Cl^- and a certain Na^+
764 neutralized the systems, and 231710 water molecules. The proteins and cofactors were
765 described by AMBER FF14SB (Maier et al., 2015) and GAFF (Wang et al., 2004) force
766 fields, respectively. MD simulations were performed using a well-established protocol
767 described elsewhere (Kim et al., 2021; Su et al., 2019; Zhang et al., 2021). Briefly, each
768 MD system was first relaxed by a series of minimizations followed by four phases of MD
769 simulations, including the relaxation phase (in total 5 nanoseconds [ns] with 1 femtosecond
770 [fs] time steps), the system heating-up phase (in total 10 ns), the equilibrium phase (10 ns),
771 and the final sampling phase (100 ns). The time step was 2 fs for the last three phases, and

the MD simulations of the last two phases were performed at 298K and 1 bar to produce isothermal-isobaric ensembles. All MD simulations were performed using the pmemd.cuda program in AMBER 18 (Case et al., 2018). Besides the root-mean-square deviation (r.m.s.d) ~ time curves, a representative MD conformation which has the smallest r.m.s.d. between itself and the average MD structure was identified for each MD system.

Free energy calculations

140 snapshots from the sampling phase (30 – 100 ns) of a trajectory were collected for free energy calculations. An internal program was applied to calculate the MM-PBSA-WSAS free energies of the complex and the binding free energy between Arf1 and WRC. The polar part of the solvation free energy was calculated using Delphi 95 software (Li et al., 2012; Rocchia et al., 2001), and the nonpolar part was estimated by scaling the solvent accessible surface area as described elsewhere (Wang et al., 2019, 2006). The conformational entropy term was predicted using WSAS, a weighted solvent-accessible surface area method (Wang and Hou, 2012). The interior and exterior dielectric constants of PBSA calculations were set to 1.0 and 80.0, respectively. To study the effect of M-site mutations, we conducted computational mutagenesis using the wildtype snapshots and calculated the MM-PBSA-WSAS free energies of complex and Arf1 binding.

Cell culture and co-immunoprecipitation

B16-F1-derived *Sra1/Cyfip2* KO cells (clone #3) were previously described (Schaks et al., 2018), and maintained in DMEM (4.5 g/l glucose; Invitrogen) supplemented with 10% FCS (Gibco), 2 mM glutamine (Thermo Fisher Scientific) and penicillin (50 Units/ml)/streptomycin (50 µg/ml) (Thermo Fisher Scientific). Cells were routinely transfected in 6 well plates (Sarstedt), using 1 µg DNA in total and 2 µl JetPrime per well.

pEGFP-C2-Sra-1 (CYFIP1) and the derived Y967A mutant construct were described previously (Schaks et al., 2018), and corresponded to the splice variant *CYFIP1a*, sequence AJ567911, of murine origin. Further point mutations in the M site were introduced by site-directed mutagenesis. The identity of all DNA constructs was verified by sequencing.

For EGFP-immunoprecipitation experiments, B16-F1-derived cell lines ectopically expressing EGFP-tagged variants of CYFIP1 were lysed with lysis buffer (1% Triton X-100, 140 mM KCl, 50 mM Tris/HCl pH 7.4 supplemented with 50 mM NaF, 10 mM $Na_4P_2O_7$, 2 mM $MgCl_2$ and Complete Mini, EDTA-free protease inhibitor [Roche]). Lysates were cleared and incubated with GFP-Trap agarose beads (Chromotek) for 60 min. Subsequently, beads were washed three times with lysis buffer lacking protease inhibitor and Triton X-100, mixed with SDS-PAGE loading buffer, boiled for 5 min, and examined by Western Blotting using primary antibodies against Sra-1/Cyfip2 (Steffen et al., 2004), Nap1 (Steffen et al., 2004), WAVE (Schaks et al., 2018) and Abi1 (D3G6C, #39444 Cell Signaling Technology), as well as corresponding, HRP-conjugated secondary antibodies (Invitrogen). Chemiluminescence signals were obtained upon incubation with ECL™ Prime Western Blotting Detection Reagent (Cytiva), and recorded with ECL Chemocam imager (Intas, Goettingen, Germany).

Fluorescence microscopy, phalloidin staining, and quantifications

B16-F1-derived cell lines expressing indicated, EGFP-tagged CYFIP1 constructs or untransfected control cells were seeded onto laminin-coated (25 µg/ml), 15 mm-diameter glass coverslips and allowed to adhere for about 24 hours prior to fixation. Cells were fixed with pre-warmed, 4% paraformaldehyde (PFA) in PBS for 20 min, and permeabilized with 0.05% Triton-X100 in PBS for 30 sec. The actin cytoskeleton was subsequently stained using

ATTO-594-conjugated phalloidin (ATTO TEC GmbH, Germany). Samples were mounted using VectaShield Vibrance antifade reagent and imaged using a 63×/1.4NA Plan apochromatic oil objective.

For assessment of lamellipodia formation, cells were randomly selected and categorized in a blinded manner as follows: "no lamellipodia" if no phalloidin-stained peripheral lamellipodia-like actin meshwork was visible, "immature lamellipodia" if the lamellipodia-like actin meshwork was small, narrow, or displayed multiple ruffles, and "lamellipodia" if the protrusive actin meshworks appeared to be fully developed (see representative examples in Figure 6A).

Statistical analysis

To assess statistical significance, one-way ANOVA with Dunnett's post-hoc test was applied to compare multiple groups with one control group. Statistical analyses were performed using Prism 6.01. An error probability below 5% ($p < 0.05$; * in Figure panels) was considered to imply statistical significance. ** and *** indicated p-values ≤ 0.01 and ≤ 0.001, respectively.

Supplemental information

Table S1. DNA constructs and WRC assemblies used in this study

Name	Description	Source/reference	Identifier
Individual proteins/subunits			
Sra1	His6-Tev-hSra1 (1-1253, full length) in pAV5a vector, His6-Tev finally removed	(Ismail et al., 2009)	pYS1
Sra1$^{D\text{-}Rac1}$	His6-Tev-Sra1-$(GGS)_4$-Rac1$^{Q61L/P29S}$ (1-188) in pAV5a vector, His6-Tev finally removed	(Ding et al., 2022)	pYS11
Sra1$^{A\text{-}Rac1}$	His6-Tev-Sra1 Y423-[$(GGS)_6$-Rac1$^{Q61L/P29S}$ (1-188)-$(GS)_6$)]-S424 (Rac1 is inserted in a loop of Sra1 between Y423/S424), in pAV5a vector, His6-Tev finally removed	This study	pYS19
Sra1$^{Y986A,\ E988A}$	986A, E988A in Sra1 (ΔM#1)	This study	pYS197
Sra1$^{Y948A,\ T951A}$	Y948A, T951A in Sra1 (ΔM#2)	This study	pYS198
Sra1$^{W845A,\ Y849A}$	W845A, Y849A in Sra1 (ΔM#3)	This study	pYS199
Sra1$^{D\text{-}PGS}$	His6-Tev-Sra1 H965-(G)-PGS-(G)-G968 (PGS is inserted between H965 and G968, with E966 and Y967 replaced by Gly), in pAV5a vector, His6-Tev finally removed (D-block)	This study	pYS110
Sra1$^{A\text{-}PGS}$	His6-Tev-Sra1 K178-(G)-PGS-(G)-S180 (PGS is inserted between K178 and S180, with C179 replaced by Gly. An extra Gly is tethered to C terminus of PGS), in pAV5a vector, His6-Tev finally removed (A-block)	This study	pYS112
Sra1^{Y967A}	Y967A in Sra1 (ΔD)	(Chen et al., 2017)	cbyd-150807-3 (AT3-1)
Sra1^{C179R}	C179R in Sra1 (ΔA)	(Chen et al., 2010)	cbyd-150807-8
Sra1$^{C179R,\ D\text{-}Rac1}$	His6-Tev-Sra1^{C179R}-$(GGS)_4$-Rac1$^{Q61L/P29S}$(1-188) in pAV5a vector, His6-Tev finally removed	This study	pYS196
Nap1	His6-Tev-hNap1 (1-1128, full length), in pAV5a vector, His6-Tev finally removed	(Ismail et al., 2009)	pYS2
WAVE1 (1-230)	MBP-Tev-hWAVE1 (1-230) in pMalC2Tev vector, MBP-Tev finally removed	(Chen et al., 2017)	pYS8
WAVE1 (1-230)-WCA	MBP-Tev-hWAVE1 (1-230)-$(GGS)_6$-WCA(485-559) in pMalC2Tev vector, MBP-Tev finally removed	(Chen et al., 2017)	pYS9
WAVE1(1-230)-Rac1	MBP-Tev-WAVE1 (1-230)-$(GGS)_6$-Rac1$^{Q61L/P29S}$ (1-188) in pMalC2Tev vector, MBP-Tev finally removed	(Chen et al., 2017)	cbyd-131103-2 (AE9-2)
Abi2 (1-158)	MBP-Tev-hAbi2 (1-158) in pMalC2Tev vector, MBP-Tev finally removed	(Ismail et al., 2009)	pYS3
HSPC300	MBP-Tev-hHSPC300 (1-79, full length) in pMalC2Tev vector, MBP-Tev finally removed	(Ismail et al., 2009)	pYS4
WCA	hWAVE1(485-559) in pET11a vector	(Ismail et al., 2009)	cbyd-090413-13 (pBC6)
GST-Arf1	GST-Thrombin-Arf1 $^{\Delta17\ (18\text{-}181)}$ in pGEX Thrombin vector	This study	pYS30
His8-Arf1	His_8-$(GGS)_2$-Arf1$^{\Delta17\ (18\text{-}181)}$ in pET11a vector	This study	pYS186
GST-Arf5	GST- Thrombin-Arf5 $^{\Delta17\ (18\text{-}180)}$ in pGEX Thrombin vector	From Neal Alto	pYS29
GST-Arf6	GST- Thrombin-Arf6 $^{\Delta13\ (14\text{-}175)}$ in pGEX Thrombin vector	From Neal Alto	pYS28
GST-Arl1	GST- Thrombin-Arl1 $^{\Delta17\ (18\text{-}181)}$ in pGEX Thrombin vector	From Neal Alto	pYS27
GST-Arl2	GST- Thrombin-Arl2 $^{\Delta13\ (14\text{-}184)}$ in pGEX Thrombin vector	From Neal Alto	pYS31

His6-EspG	His_6-EspG$^{\Delta 41\ (42\text{-}398)}$ in pPROEX HTb vector	From Neal Alto	pYS70
GST-Rac1^{QP}	GST-Tev-Rac1$^{Q61L/P29S}$(1-188) in pGEXTev vector	(Chen et al., 2017)	pYS7
GST-Rac1^{dead}	Switch I (a.a. 25-39) replaced by $(GGS)_5$ in GST-Rac1	This study	pYS107
Untagged Rac1 ^{QP}	Rac1$^{Q61L/P29S}$(1-188) in pET11a vector	(Chen et al., 2017)	pYS108
EGFP-mCyfip1	EGFP-mCyfip1 in pEGFP vector	(Schaks et al., 2018)	pMS1
EGFP-mCyfip1^{Y967A}	EGFP-mCyfip1^{Y967A} in pEGFP vector (ΔD)	(Schaks et al., 2018)	pMS5
EGFP-mCyfip1$^{Y986A, E988A}$	EGFP-mCyfip1$^{Y986A, E988A}$ in pEGFP vector (ΔM#1)	This study	pMS140
EGFP-mCyfip1$^{Y948A, T951A}$	EGFP-mCyfip1$^{Y948A, T951A}$ in pEGFP vector (ΔM#2)	This study	pMS141
EGFP-mCyfip1$^{Y967A, Y986A, E988A}$	EGFP-mCyfip1$^{Y967A, Y986A, E988A}$ in pEGFP vector (ΔD, ΔM#1)	This study	pMS156
EGFP-mCyfip1$^{Y967A, Y948A, T951A}$	EGFP-mCyfip1$^{Y967A, Y948A, T951A}$ in pEGFP vector (ΔD, ΔM#2)	This study	pMS157
Assembled WRC (refer to the above table for subunit information)			
WRC^{230WCA}, or WRC^{apo}	Sra1, Nap1, WAVE1 (1-230)-WCA, Abi2 (1-158), and HSPC300	(Chen et al., 2017)	WRC^{230WCA}, or WRC^{apo}
WRC$^{D\text{-}Rac1}$	Sra1$^{D\text{-}Rac1}$, Nap1, WAVE1 (1-230)-WCA, Abi2 (1-158), and HSPC300	(Ding et al., 2022)	WRC$^{D\text{-}Rac1}$
WRC$^{\Delta A, D\text{-}Rac1}$	Sra1$^{C179R, D\text{-}Rac1}$, Nap1, WAVE1 (1-230)-WCA, Abi2 (1-158), and HSPC300	This study	WRC$^{\Delta A, D\text{-}Rac1}$
WRC$^{\Delta M\#1}$	Sra1$^{Y986A, E988A}$, Nap1, WAVE1 (1-230)-WCA, Abi2 (1-158), and HSPC300	This study	WRC$^{\Delta M\#1}$
WRC$^{\Delta M\#2}$	Sra1$^{Y948A, T951A}$, Nap1, WAVE1 (1-230)-WCA, Abi2 (1-158), and HSPC300	This study	WRC$^{\Delta M\#2}$
ΔWRC230	Sra1, Nap1, WAVE1 (1-230), Abi2 (1-158), and HSPC300	(Chen et al., 2017)	ΔWRC230
ΔWRC230$^{D\text{-}Rac1}$	Sra1$^{D\text{-}Rac1}$, Nap1, WAVE1 (1-230), Abi2 (1-158), and HSPC300	(Ding et al., 2022)	ΔWRC230$^{D\text{-}Rac1}$
ΔWRC230$^{A\text{-}Rac1}$	Sra1$^{A\text{-}Rac1}$, Nap1, WAVE1 (1-230), Abi2 (1-158), and HSPC300	This study	ΔWRC230$^{A\text{-}Rac1}$
ΔWRC230$^{\Delta WCA\text{-}Rac1}$	Sra1, Nap1, WAVE1(1-230)-Rac1, Abi2 (1-158), and HSPC300	(Chen et al., 2017)	ΔWRC230$^{\Delta WCA\text{-}Rac1}$
ΔWRC230$^{D\text{-}block}$	Sra1$^{D\text{-}PGS}$, Nap1, WAVE1 (1-230), Abi2 (1-158), and HSPC300	This study	ΔWRC230$^{D\text{-}block}$
ΔWRC230$^{A\text{-}block}$	Sra1$^{A\text{-}PGS}$, Nap1, WAVE1 (1-230), Abi2 (1-158), and HSPC300	This study	ΔWRC230$^{A\text{-}block}$
ΔWRC230$^{\Delta M\#1}$	Sra1$^{Y986A, E988A}$, Nap1, WAVE1 (1-230)-WCA, Abi2 (1-158), and HSPC300	This study	ΔWRC230$^{\Delta M\#1}$
ΔWRC230$^{\Delta M\#2}$	Sra1$^{Y948A, T951A}$, Nap1, WAVE1 (1-230)-WCA, Abi2 (1-158), and HSPC300	This study	ΔWRC230$^{\Delta M\#2}$
ΔWRC230$^{\Delta M\#3}$	Sra1$^{W845A, Y849A}$, Nap1, WAVE1 (1-230)-WCA, Abi2 (1-158), and HSPC300	This study	ΔWRC230$^{\Delta M\#3}$

836

837

838 **Table S2. Sequences of recombinant proteins used in this study**

839 Only sequences in the final product (i.e., after protease cleavage to remove the affinity

840 tag) are shown and are annotated by corresponding colors.

841

>**Sra1** GAMAAQVTLEDALSNVDLLEELPLPDQQPCIEPPPSSLLYQPNFNTNFEDRNAFVTGIARYIEQATVHSSMNEMLEEGQE YAVMLYTWRSCSRAIPQVKCNEQPNRVEIYEKTVEVLEPEVTKLMNFMYFQRNAIERFCGEVRRLCHAERRKDFVSEAY LITLGKFINMFAVLDELKNMKCSVKNDHSAYKRAAQFLRKMADPQSIQESQNLSMFLANHNKITQSLQQQLEVISGYEEL LADIVNLCVDYYENRMYLTPSEKHMLLKVMGFGLYLMDGSVSNIYKLDAKKRINLSKIDKYFKQLQVVPLFGDMQIELA RYIKTSAHYEENKSRWTCTSSGSSPQYNICEQMIQIREDHMRFISELARYSNSEVVTGSGRQEAQKTDAEYRKLFDLALQG LQLLSQWSAHVMEVYSWKLVHPTDKYSNKDCPDSAEEYERATRYNYTSEEKFALVEVIAMIKGLQVLMGRMESVFNH AIRHTVYAALQDFSQVTLREPLRQAIKKKKNVIQSVLQAIRKTVCDWETGHEPFNDPALRGEKDPKSGFDIKVPRRAVGP SSTQLYMVRTMLESLIADKSGSKKTLRSSLEGPTILDIEKFHRESFFYTHLINFSETLQQCCDLSQLWFREFFLELTMGRRIQ FPIEMSMPWILTDHILETKEASMMEYVLYSLDLYNDSAHYALTRFNKQFLYDEIEAEVNLCFDQFVYKLADQIFAYYKV MAGSLLLDKRLRSECKNQGATIHLPPSNRYETLLKQRHVQLLGRSIDLNRLITQRVSAAMYKSLELAIGRFESEDLTSIVEL DGLLEINRMTHKLLSRYLTLDGFDAMFREANHNVSAPYGRITLHVFWELNYDFLPNYCYNGSTNRFVRTVLPFSQEFQR DKQPNAQPQYLHGSKALNLAYSSIYGSYRNFVGPPHFQVICRLLGYQGIAVVMEELLKVVKSLLQGTILQYVKTLMEVM PKICRLPRHEYGSPGILEFFHHQLKDIVEYAELKTVCFQNLREVGNAILFCLLIEQSLSLEEVCDLLHAAPFQNILPRVHVKE GERLDAKMKRLESKYAPLHLVPLIERLGTPQQIAIAREGDLLTKERLCCGLSMFEVILTRIRSFLDDPIWRGPLPSNGVMH VDECVEFHRLWSAMQFVYCIPVGTHEFTVEQCFGDGLHWAGCMIIVLLGQQRRFAVLDFCYHLLKVQKHDGKDEIIKNV PLKKMVERIRKFQILNDEIITILDKYLKSGDGEGTPVEHVRCFQPPIHQSLASS
>**Sra1**$^{\text{D-Rac1}}$, or **Sra1-**$(GGS)_4$**-Rac1**$^{\text{Q61L/P29S}}$**(1-188)** GAMAAQVTLEDALSNVDLLEELPLPDQQPCIEPPPSSLLYQPNFNTNFEDRNAFVTGIARYIEQATVHSSMNEMLEEGQE YAVMLYTWRSCSRAIPQVKCNEQPNRVEIYEKTVEVLEPEVTKLMNFMYFQRNAIERFCGEVRRLCHAERRKDFVSEAY LITLGKFINMFAVLDELKNMKCSVKNDHSAYKRAAQFLRKMADPQSIQESQNLSMFLANHNKITQSLQQQLEVISGYEEL LADIVNLCVDYYENRMYLTPSEKHMLLKVMGFGLYLMDGSVSNIYKLDAKKRINLSKIDKYFKQLQVVPLFGDMQIELA RYIKTSAHYEENKSRWTCTSSGSSPQYNICEQMIQIREDHMRFISELARYSNSEVVTGSGRQEAQKTDAEYRKLFDLALQG LQLLSQWSAHVMEVYSWKLVHPTDKYSNKDCPDSAEEYERATRYNYTSEEKFALVEVIAMIKGLQVLMGRMESVFNH AIRHTVYAALQDFSQVTLREPLRQAIKKKKNVIQSVLQAIRKTVCDWETGHEPFNDPALRGEKDPKSGFDIKVPRRAVGP SSTQLYMVRTMLESLIADKSGSKKTLRSSLEGPTILDIEKFHRESFFYTHLINFSETLQQCCDLSQLWFREFFLELTMGRRIQ FPIEMSMPWILTDHILETKEASMMEYVLYSLDLYNDSAHYALTRFNKQFLYDEIEAEVNLCFDQFVYKLADQIFAYYKV MAGSLLLDKRLRSECKNQGATIHLPPSNRYETLLKQRHVQLLGRSIDLNRLITQRVSAAMYKSLELAIGRFESEDLTSIVEL DGLLEINRMTHKLLSRYLTLDGFDAMFREANHNVSAPYGRITLHVFWELNYDFLPNYCYNGSTNRFVRTVLPFSQEFQR DKQPNAQPQYLHGSKALNLAYSSIYGSYRNFVGPPHFQVICRLLGYQGIAVVMEELLKVVKSLLQGTILQYVKTLMEVM PKICRLPRHEYGSPGILEFFHHQLKDIVEYAELKTVCFQNLREVGNAILFCLLIEQSLSLEEVCDLLHAAPFQNILPRVHVKE GERLDAKMKRLESKYAPLHLVPLIERLGTPQQIAIAREGDLLTKERLCCGLSMFEVILTRIRSFLDDPIWRGPLPSNGVMH VDECVEFHRLWSAMQFVYCIPVGTHEFTVEQCFGDGLHWAGCMIIVLLGQQRRFAVLDFCYHLLKVQKHDGKDEIIKNV PLKKMVERIRKFQILNDEIITILDKYLKSGDGEGTPVEHVRCFQPPIHQSLASS**GGSGGSGGSGGS**MQAIKCVVVGDGAV GKTCLLISYTTNAF**S**GEYIPTVFDNYSANVMVDGKPVNLGLWDTAG**L**EDYDRLRPLSYPQTDVFLICFSLVSPASFENVR AKWYPEVRHHCPNTPIILVGTKLDLRDDKDTIEKLKEKKLTPITYPQGLAMAKEIGAVKYLECSALTQRGLKTVFDEAIR AVLCPPPVKKRKRK
>**Sra1**$^{\text{A-Rac1}}$ or **Sra1 Y423-[**$(GGS)_6$**-Rac1**$^{\text{Q61L/P29S}}$**(1-188)-**$(GS)_6$**)]-S424** GAMAAQVTLEDALSNVDLLEELPLPDQQPCIEPPPSSLLYQPNFNTNFEDRNAFVTGIARYIEQATVHSSMNEMLEEGQE YAVMLYTWRSCSRAIPQVKCNEQPNRVEIYEKTVEVLEPEVTKLMNFMYFQRNAIERFCGEVRRLCHAERRKDFVSEAY LITLGKFINMFAVLDELKNMKCSVKNDHSAYKRAAQFLRKMADPQSIQESQNLSMFLANHNKITQSLQQQLEVISGYEEL LADIVNLCVDYYENRMYLTPSEKHMLLKVMGFGLYLMDGSVSNIYKLDAKKRINLSKIDKYFKQLQVVPLFGDMQIELA RYIKTSAHYEENKSRWTCTSSGSSPQYNICEQMIQIREDHMRFISELARYSNSEVVTGSGRQEAQKTDAEYRKLFDLALQG LQLLSQWSAHVMEVYSWKLVHPTDKY**GGSGGSGGSGGSGGSGGS**MQAIKCVVVGDGAVGKTCLLISYTTNAF**S**GEYI PTVFDNYSANVMVDGKPVNLGLWDTAG**L**EDYDRLRPLSYPQTDVFLICFSLVSPASFENVRAKWYPEVRHHCPNTPIILV GTKLDLRDDKDTIEKLKEKKLTPITYPQGLAMAKEIGAVKYLECSALTQRGLKTVFDEAIRAVLCPPPVKKRKRK**GSGSG** **SGSGSGS**SNKDCPDSAEEYERATRYNYTSEEKFALVEVIAMIKGLQVLMGRMESVFNHAIRHTVYAALQDFSQVTLREP LRQAIKKKKNVIQSVLQAIRKTVCDWETGHEPFNDPALRGEKDPKSGFDIKVPRRAVGPSSTQLYMVRTMLESLIADKSG SKKTLRSSLEGPTILDIEKFHRESFFYTHLINFSETLQQCCDLSQLWFREFFLELTMGRRIQFPIEMSMPWILTDHILETKEAS MMEYVLYSLDLYNDSAHYALTRFNKQFLYDEIEAEVNLCFDQFVYKLADQIFAYYKVMAGSLLLDKRLRSECKNQGAT IHLPPSNRYETLLKQRHVQLLGRSIDLNRLITQRVSAAMYKSLELAIGRFESEDLTSIVELDGLLEINRMTHKLLSRYLTLD GFDAMFREANHNVSAPYGRITLHVFWELNYDFLPNYCYNGSTNRFVRTVLPFSQEFQRDKQPNAQPQYLHGSKALNLA YSSIYGSYRNFVGPPHFQVICRLLGYQGIAVVMEELLKVVKSLLQGTILQYVKTLMEVMPKICRLPRHEYGSPGILEFFHH QLKDIVEYAELKTVCFQNLREVGNAILFCLLIEQSLSLEEVCDLLHAAPFQNILPRVHVKEGERLDAKMKRLESKYAPLHL VPLIERLGTPQQIAIAREGDLLTKERLCCGLSMFEVILTRIRSFLDDPIWRGPLPSNGVMHVDECVEFHRLWSAMQFVYCIP VGTHEFTVEQCFGDGLHWAGCMIIVLLGQQRRFAVLDFCYHLLKVQKHDGKDEIIKNVPLKKMVERIRKFQILNDEIITIL DKYLKSGDGEGTPVEHVRCFQPPIHQSLASS

> **Sra1**$^{Y986A,\ E988A}$

GAMAAQVTLEDALSNVDLLEELPLPDQQPCIEPPPSSLLYQPNFNTNFEDRNAFVTGIARYIEQATVHSSMNEMLEEGQE
YAVMLYTWRSCSRAIPQVKCNEQPNRVEIYEKTVEVLEPEVTKLMNFMYFQRNAIERFCGEVRRLCHAERRKDFVSEAY
LITLGKFINMFAVLDELKNMKCSVKNDHSAYKRAAQFLRKMADPQSIQESQNLSMFLANHNKITQSLQQQLEVISGYEEL
LADIVNLCVDYYENRMYLTPSEKHMLLKVMGFGLYLMDGSVSNIYKLDAKKRINLSKIDKYFKQLQVVPLFGDMQIELA
RYIKTSAHYEENKSRWTCTSSGSSPQYNICEQMIQIREDHMRFISELARYSNSEVVTGSGRQEAQKTDAEYRKLFDLALQG
LQLLSQWSAHVMEVYSWKLVHPTDKYSNKDCPDSAEEYERATRYNYTSEEKFALVEVIAMIKGLQVLMGRMESVFNH
AIRHTVYAALQDFSQVTLREPLRQAIKKKKNVIQSVLQAIRKTVCDWETGHEPFNDPALRGEKDPKSGFDIKVPRRAVGP
SSTQLYMVRTMLESLIADKSGSKKTLRSSLEGPTILDIEKFHRESFFYTHLINFSETLQQCCDLSQLWFREFFLELTMGRRIQ
FPIEMSMPWILTDHILETKEASMMEYVLYSLDLYNDSAHYALTRFNKQFLYDEIEAEVNLCFDQFVYKLADQIFAYYKV
MAGSLLLDKRLRSECKNQGATIHLPPSNRYETLLKQRHVQLLGRSIDLNRLITQRVSAAMYKSLELAIGRFESEDLTSIVEL
DGLLEINRMTHKLLSRYLTLDGFDAMFREANHNVSAPYGRITLHVFWELNYDFLPNYCYNGSTNRFVRTVLPFSQEFQR
DKQPNAQPQYLHGSKALNLAYSSIYGSYRNFVGPPHFQVICRLLGYQGIAVVMEELLKVVKSLLQGTILQYVKTLMEVM
PKICRLPRHEYGSPGILEFFHHQLKDIVE**A**A**A**LKTVCFQNLREVGNAILFCLLIEQSLSLEEVCDLLHAAPFQNILPRVHVKE
GERLDAKMKRLESKYAPLHLVPLIERLGTPQQIAIAREGDLLTKERLCCGLSMFEVILTRIRSFLDDPIWRGPLPSNGVMH
VDECVEFHRLWSAMQFVYCIPVGTHEFTVEQCFGDGLHWAGCMIIVLLGQQRRFAVLDFCYHLLKVQKHDGKDEIIKNV
PLKKMVERIRKFQILNDEIITILDKYLKSGDGEGTPVEHVRCFQPPIHQSLASS

> **Sra1**$^{Y948A,\ T951A}$

GAMAAQVTLEDALSNVDLLEELPLPDQQPCIEPPPSSLLYQPNFNTNFEDRNAFVTGIARYIEQATVHSSMNEMLEEGQE
YAVMLYTWRSCSRAIPQVKCNEQPNRVEIYEKTVEVLEPEVTKLMNFMYFQRNAIERFCGEVRRLCHAERRKDFVSEAY
LITLGKFINMFAVLDELKNMKCSVKNDHSAYKRAAQFLRKMADPQSIQESQNLSMFLANHNKITQSLQQQLEVISGYEEL
LADIVNLCVDYYENRMYLTPSEKHMLLKVMGFGLYLMDGSVSNIYKLDAKKRINLSKIDKYFKQLQVVPLFGDMQIELA
RYIKTSAHYEENKSRWTCTSSGSSPQYNICEQMIQIREDHMRFISELARYSNSEVVTGSGRQEAQKTDAEYRKLFDLALQG
LQLLSQWSAHVMEVYSWKLVHPTDKYSNKDCPDSAEEYERATRYNYTSEEKFALVEVIAMIKGLQVLMGRMESVFNH
AIRHTVYAALQDFSQVTLREPLRQAIKKKKNVIQSVLQAIRKTVCDWETGHEPFNDPALRGEKDPKSGFDIKVPRRAVGP
SSTQLYMVRTMLESLIADKSGSKKTLRSSLEGPTILDIEKFHRESFFYTHLINFSETLQQCCDLSQLWFREFFLELTMGRRIQ
FPIEMSMPWILTDHILETKEASMMEYVLYSLDLYNDSAHYALTRFNKQFLYDEIEAEVNLCFDQFVYKLADQIFAYYKV
MAGSLLLDKRLRSECKNQGATIHLPPSNRYETLLKQRHVQLLGRSIDLNRLITQRVSAAMYKSLELAIGRFESEDLTSIVEL
DGLLEINRMTHKLLSRYLTLDGFDAMFREANHNVSAPYGRITLHVFWELNYDFLPNYCYNGSTNRFVRTVLPFSQEFQR
DKQPNAQPQYLHGSKALNLAYSSIYGSYRNFVGPPHFQVICRLLGYQGIAVVMEELLKVVKSLLQGTILQ**A**VK**A**LMEVM
PKICRLPRHEYGSPGILEFFHHQLKDIVEYAELKTVCFQNLREVGNAILFCLLIEQSLSLEEVCDLLHAAPFQNILPRVHVKE
GERLDAKMKRLESKYAPLHLVPLIERLGTPQQIAIAREGDLLTKERLCCGLSMFEVILTRIRSFLDDPIWRGPLPSNGVMH
VDECVEFHRLWSAMQFVYCIPVGTHEFTVEQCFGDGLHWAGCMIIVLLGQQRRFAVLDFCYHLLKVQKHDGKDEIIKNV
PLKKMVERIRKFQILNDEIITILDKYLKSGDGEGTPVEHVRCFQPPIHQSLASS

> **Sra1**$^{W845A,\ Y849A}$

GAMAAQVTLEDALSNVDLLEELPLPDQQPCIEPPPSSLLYQPNFNTNFEDRNAFVTGIARYIEQATVHSSMNEMLEEGQE
YAVMLYTWRSCSRAIPQVKCNEQPNRVEIYEKTVEVLEPEVTKLMNFMYFQRNAIERFCGEVRRLCHAERRKDFVSEAY
LITLGKFINMFAVLDELKNMKCSVKNDHSAYKRAAQFLRKMADPQSIQESQNLSMFLANHNKITQSLQQQLEVISGYEEL
LADIVNLCVDYYENRMYLTPSEKHMLLKVMGFGLYLMDGSVSNIYKLDAKKRINLSKIDKYFKQLQVVPLFGDMQIELA
RYIKTSAHYEENKSRWTCTSSGSSPQYNICEQMIQIREDHMRFISELARYSNSEVVTGSGRQEAQKTDAEYRKLFDLALQG
LQLLSQWSAHVMEVYSWKLVHPTDKYSNKDCPDSAEEYERATRYNYTSEEKFALVEVIAMIKGLQVLMGRMESVFNH
AIRHTVYAALQDFSQVTLREPLRQAIKKKKNVIQSVLQAIRKTVCDWETGHEPFNDPALRGEKDPKSGFDIKVPRRAVGP
SSTQLYMVRTMLESLIADKSGSKKTLRSSLEGPTILDIEKFHRESFFYTHLINFSETLQQCCDLSQLWFREFFLELTMGRRIQ
FPIEMSMPWILTDHILETKEASMMEYVLYSLDLYNDSAHYALTRFNKQFLYDEIEAEVNLCFDQFVYKLADQIFAYYKV
MAGSLLLDKRLRSECKNQGATIHLPPSNRYETLLKQRHVQLLGRSIDLNRLITQRVSAAMYKSLELAIGRFESEDLTSIVEL
DGLLEINRMTHKLLSRYLTLDGFDAMFREANHNVSAPYGRITLHVF**A**ELN**A**DFLPNYCYNGSTNRFVRTVLPFSQEFQRD
KQPNAQPQYLHGSKALNLAYSSIYGSYRNFVGPPHFQVICRLLGYQGIAVVMEELLKVVKSLLQGTILQYVKTLMEVMP
KICRLPRHEYGSPGILEFFHHQLKDIVEYAELKTVCFQNLREVGNAILFCLLIEQSLSLEEVCDLLHAAPFQNILPRVHVKE
GERLDAKMKRLESKYAPLHLVPLIERLGTPQQIAIAREGDLLTKERLCCGLSMFEVILTRIRSFLDDPIWRGPLPSNGVMH
VDECVEFHRLWSAMQFVYCIPVGTHEFTVEQCFGDGLHWAGCMIIVLLGQQRRFAVLDFCYHLLKVQKHDGKDEIIKNV
PLKKMVERIRKFQILNDEIITILDKYLKSGDGEGTPVEHVRCFQPPIHQSLASS

>**Sra1**$^{D\text{-}PGS}$ or **Sra1 H965-(G)-PGS-(G)-G968**

GAMAAQVTLEDALSNVDLLEELPLPDQQPCIEPPPSSLLYQPNFNTNFEDRNAFVTGIARYIEQATVHSSMNEMLEEGQE
YAVMLYTWRSCSRAIPQVKCNEQPNRVEIYEKTVEVLEPEVTKLMNFMYFQRNAIERFCGEVRRLCHAERRKDFVSEAY
LITLGKFINMFAVLDELKNMKCSVKNDHSAYKRAAQFLRKMADPQSIQESQNLSMFLANHNKITQSLQQQLEVISGYEEL
LADIVNLCVDYYENRMYLTPSEKHMLLKVMGFGLYLMDGSVSNIYKLDAKKRINLSKIDKYFKQLQVVPLFGDMQIELA
RYIKTSAHYEENKSRWTCTSSGSSPQYNICEQMIQIREDHMRFISELARYSNSEVVTGSGRQEAQKTDAEYRKLFDLALQG
LQLLSQWSAHVMEVYSWKLVHPTDKYSNKDCPDSAEEYERATRYNYTSEEKFALVEVIAMIKGLQVLMGRMESVFNH
AIRHTVYAALQDFSQVTLREPLRQAIKKKKNVIQSVLQAIRKTVCDWETGHEPFNDPALRGEKDPKSGFDIKVPRRAVGP
SSTQLYMVRTMLESLIADKSGSKKTLRSSLEGPTILDIEKFHRESFFYTHLINFSETLQQCCDLSQLWFREFFLELTMGRRIQ
FPIEMSMPWILTDHILETKEASMMEYVLYSLDLYNDSAHYALTRFNKQFLYDEIEAEVNLCFDQFVYKLADQIFAYYKV
MAGSLLLDKRLRSECKNQGATIHLPPSNRYETLLKQRHVQLLGRSIDLNRLITQRVSAAMYKSLELAIGRFESEDLTSIVEL
DGLLEINRMTHKLLSRYLTLDGFDAMFREANHNVSAPYGRITLHVFWELNYDFLPNYCYNGSTNRFVRTVLPFSQEFQR
DKQPNAQPQYLHGSKALNLAYSSIYGSYRNFVGPPHFQVICRLLGYQGIAVVMEELLKVVKSLLQGTILQYVKTLMEVM
PKICRLPRH**G**GIDCSFWNESYLTGSRDERKKSLLSKFGMDEGVTFMFIGRFDRGQKGVDVLLKAIEILSSKKEFQEMRFIII
GKGDPELEGWARSLEEKHGNVKVITEMLSREFVRELYGSVDFVIIPSYFEPFGLVALEAMCLGAIPIASAVGGLRDIITNET
GILVKAGDPGELANAILKALELSRSDLSKFRENCKKRAMSFS**G**GSPGILEFFHHQLKDIVEYAELKTVCFQNLREVGNAIL

FCLLIEQSLSLEEVCDLLHAAPFQNILPRVHVKEGERLDAKMKRLESKYAPLHLVPLIERLGTPQQIAIAREGDLLTKERLC
CGLSMFEVILTRIRSFLDDPIWRGPLPSNGVMHVDECVEFHRLWSAMQFVYCIPVGTHEFTVEQCFGDGLHWAGCMIIVL
LGQQRRFAVLDFCYHLLKVQKHDGKDEIIKNVPLKKMVERIRKFQILNDEIITILDKYLKSGDGEGTPVEHVRCFQPPIHQS
LASS

>**Sra1**$^{A\text{-}PGS}$ or **K178-(G)-PGS-(G)-S180**
GAMAAQVTLEDALSNVDLLEELPLPDQQPCIEPPPSSLLYQPNFNTNFEDRNAFVTGIARYIEQATVHSSMNEMLEEGQE
YAVMLYTWRSCSRAIPQVKCNEQPNRVEIYEKTVEVLEPEVTKLMNFMYFQRNAIERFCGEVRRLCHAERRKDFVSEAY
LITLGKFINMFAVLDELKNMK**G**GIDCSFWNESYLTGSRDERKKSLLSKFGMDEGVTFMFIGRFDRGQKGVDVLLKAIEIL
SSKKEFQEMRFIIIGKGDPELEGWARSLEEKHGNVKVITEMLSREFVRELYGSVDFVIIPSYFEPFGLVALEAMCLGAIPIAS
AVGGLRDIITNETGILVKAGDPGELANAILKALELSRSDLSKFRENCKKRAMSFS**G**SVKNDHSAYKRAAQFLRKMADPQS
IQESQNLSMFLANHNKITQSLQQQLEVISGYEELLADIVNLCVDYYENRMYLTPSEKHMLLKVMGFGLYLMDGSVSNIY
KLDAKKRINLSKIDKYFKQLQVVPLFGDMQIELARYIKTSAHYEENKSRWTCTSSGSSPQYNICEQMIQIREDHMRFISEL
ARYSNSEVVTGSGRQEAQKTDAEYRKLFDLALQGLQLLSQWSAHVMEVYSWKLVHPTDKYSNKDCPDSAEEYERATR
YNYTSEEKFALVEVIAMIKGLQVLMGRMESVFNHAIRHTVYAALQDFSQVTLREPLRQAIKKKKNVIQSVLQAIRKTVCD
WETGHEPFNDPALRGEKDPKSGFDIKVPRRAVGPSSTQLYMVRTMLESLIADKSGSKKTLRSSLEGPTILDIEKFHRESFFY
THLINFSETLQQCCDLSQLWFREFFLELTMGRRIQFPIEMSMPWILTDHILETKEASMMEYVLYSLDLYNDSAHYALTRFN
KQFLYDEIEAEVNLCFDQFVYKLADQIFAYYKVMAGSLLLDKRLRSECKNQGATIHLPPSNRYETLLKQRHVQLLGRSID
LNRLITQRVSAAMYKSLELAIGRFESEDLTSIVELDGLLEINRMTHKLLSRYLTLDGFDAMFREANHNVSAPYGRITLHVF
WELNYDFLPNYCYNGSTNRFVRTVLPFSQEFQRDKQPNAQPQYLHGSKALNLAYSSIYGSYRNFVGPPHFQVICRLLGYQ
GIAVVMEELLKVVKSLLQGTILQYVKTLMEVMPKICRLPRHEYGSPGILEFFHHQLKDIVEYAELKTVCFQNLREVGNAIL
FCLLIEQSLSLEEVCDLLHAAPFQNILPRVHVKEGERLDAKMKRLESKYAPLHLVPLIERLGTPQQIAIAREGDLLTKERLC
CGLSMFEVILTRIRSFLDDPIWRGPLPSNGVMHVDECVEFHRLWSAMQFVYCIPVGTHEFTVEQCFGDGLHWAGCMIIVL
LGQQRRFAVLDFCYHLLKVQKHDGKDEIIKNVPLKKMVERIRKFQILNDEIITILDKYLKSGDGEGTPVEHVRCFQPPIHQS
LASS

>**Sra1**^{Y967A}
GAMAAQVTLEDALSNVDLLEELPLPDQQPCIEPPPSSLLYQPNFNTNFEDRNAFVTGIARYIEQATVHSSMNEMLEEGQE
YAVMLYTWRSCSRAIPQVKCNEQPNRVEIYEKTVEVLEPEVTKLMNFMYFQRNAIERFCGEVRRLCHAERRKDFVSEAY
LITLGKFINMFAVLDELKNMKCSVKNDHSAYKRAAQFLRKMADPQSIQESQNLSMFLANHNKITQSLQQQLEVISGYEEL
LADIVNLCVDYYENRMYLTPSEKHMLLKVMGFGLYLMDGSVSNIYKLDAKKRINLSKIDKYFKQLQVVPLFGDMQIELA
RYIKTSAHYEENKSRWTCTSSGSSPQYNICEQMIQIREDHMRFISELARYSNSEVVTGSGRQEAQKTDAEYRKLFDLALQG
LQLLSQWSAHVMEVYSWKLVHPTDKYSNKDCPDSAEEYERATRYNYTSEEKFALVEVIAMIKGLQVLMGRMESVFNH
AIRHTVYAALQDFSQVTLREPLRQAIKKKKNVIQSVLQAIRKTVCDWETGHEPFNDPALRGEKDPKSGFDIKVPRRAVGP
SSTQLYMVRTMLESLIADKSGSKKTLRSSLEGPTILDIEKFHRESFFYTHLINFSETLQQCCDLSQLWFREFFLELTMGRRIQ
FPIEMSMPWILTDHILETKEASMMEYVLYSLDLYNDSAHYALTRFNKQFLYDEIEAEVNLCFDQFVYKLADQIFAYYKV
MAGSLLLDKRLRSECKNQGATIHLPPSNRYETLLKQRHVQLLGRSIDLNRLITQRVSAAMYKSLELAIGRFESEDLTSIVEL
DGLLEINRMTHKLLSRYLTLDGFDAMFREANHNVSAPYGRITLHVFWELNYDFLPNYCYNGSTNRFVRTVLPFSQEFQR
DKQPNAQPQYLHGSKALNLAYSSIYGSYRNFVGPPHFQVICRLLGYQGIAVVMEELLKVVKSLLQGTILQYVKTLMEVM
PKICRLPRHE**A**GSPGILEFFHHQLKDIVEYAELKTVCFQNLREVGNAILFCLLIEQSLSLEEVCDLLHAAPFQNILPRVHVKE
GERLDAKMKRLESKYAPLHLVPLIERLGTPQQIAIAREGDLLTKERLCCGLSMFEVILTRIRSFLDDPIWRGPLPSNGVMH
VDECVEFHRLWSAMQFVYCIPVGTHEFTVEQCFGDGLHWAGCMIIVLLGQQRRFAVLDFCYHLLKVQKHDGKDEIIKNV
PLKKMVERIRKFQILNDEIITILDKYLKSGDGEGTPVEHVRCFQPPIHQSLASS

>**Sra1**^{C179R}
GAMAAQVTLEDALSNVDLLEELPLPDQQPCIEPPPSSLLYQPNFNTNFEDRNAFVTGIARYIEQATVHSSMNEMLEEGQE
YAVMLYTWRSCSRAIPQVKCNEQPNRVEIYEKTVEVLEPEVTKLMNFMYFQRNAIERFCGEVRRLCHAERRKDFVSEAY
LITLGKFINMFAVLDELKNMK**R**SVKNDHSAYKRAAQFLRKMADPQSIQESQNLSMFLANHNKITQSLQQQLEVISGYEEL
LADIVNLCVDYYENRMYLTPSEKHMLLKVMGFGLYLMDGSVSNIYKLDAKKRINLSKIDKYFKQLQVVPLFGDMQIELA
RYIKTSAHYEENKSRWTCTSSGSSPQYNICEQMIQIREDHMRFISELARYSNSEVVTGSGRQEAQKTDAEYRKLFDLALQG
LQLLSQWSAHVMEVYSWKLVHPTDKYSNKDCPDSAEEYERATRYNYTSEEKFALVEVIAMIKGLQVLMGRMESVFNH
AIRHTVYAALQDFSQVTLREPLRQAIKKKKNVIQSVLQAIRKTVCDWETGHEPFNDPALRGEKDPKSGFDIKVPRRAVGP
SSTQLYMVRTMLESLIADKSGSKKTLRSSLEGPTILDIEKFHRESFFYTHLINFSETLQQCCDLSQLWFREFFLELTMGRRIQ
FPIEMSMPWILTDHILETKEASMMEYVLYSLDLYNDSAHYALTRFNKQFLYDEIEAEVNLCFDQFVYKLADQIFAYYKV
MAGSLLLDKRLRSECKNQGATIHLPPSNRYETLLKQRHVQLLGRSIDLNRLITQRVSAAMYKSLELAIGRFESEDLTSIVEL
DGLLEINRMTHKLLSRYLTLDGFDAMFREANHNVSAPYGRITLHVFWELNYDFLPNYCYNGSTNRFVRTVLPFSQEFQR
DKQPNAQPQYLHGSKALNLAYSSIYGSYRNFVGPPHFQVICRLLGYQGIAVVMEELLKVVKSLLQGTILQYVKTLMEVM
PKICRLPRHEYGSPGILEFFHHQLKDIVEYAELKTVCFQNLREVGNAILFCLLIEQSLSLEEVCDLLHAAPFQNILPRVHVKE
GERLDAKMKRLESKYAPLHLVPLIERLGTPQQIAIAREGDLLTKERLCCGLSMFEVILTRIRSFLDDPIWRGPLPSNGVMH
VDECVEFHRLWSAMQFVYCIPVGTHEFTVEQCFGDGLHWAGCMIIVLLGQQRRFAVLDFCYHLLKVQKHDGKDEIIKNV
PLKKMVERIRKFQILNDEIITILDKYLKSGDGEGTPVEHVRCFQPPIHQSLASS

>**Sra1**$^{C179R,\ D\text{-}Rac1}$, or **Sra1**^{C179R} **-(GGS)$_4$-Rac1**$^{Q61L/P29S}$**(1-188)**
GAMAAQVTLEDALSNVDLLEELPLPDQQPCIEPPPSSLLYQPNFNTNFEDRNAFVTGIARYIEQATVHSSMNEMLEEGQE
YAVMLYTWRSCSRAIPQVKCNEQPNRVEIYEKTVEVLEPEVTKLMNFMYFQRNAIERFCGEVRRLCHAERRKDFVSEAY
LITLGKFINMFAVLDELKNMK**R**SVKNDHSAYKRAAQFLRKMADPQSIQESQNLSMFLANHNKITQSLQQQLEVISGYEEL
LADIVNLCVDYYENRMYLTPSEKHMLLKVMGFGLYLMDGSVSNIYKLDAKKRINLSKIDKYFKQLQVVPLFGDMQIELA
RYIKTSAHYEENKSRWTCTSSGSSPQYNICEQMIQIREDHMRFISELARYSNSEVVTGSGRQEAQKTDAEYRKLFDLALQG
LQLLSQWSAHVMEVYSWKLVHPTDKYSNKDCPDSAEEYERATRYNYTSEEKFALVEVIAMIKGLQVLMGRMESVFNH
AIRHTVYAALQDFSQVTLREPLRQAIKKKKNVIQSVLQAIRKTVCDWETGHEPFNDPALRGEKDPKSGFDIKVPRRAVGP

SSTQLYMVRTMLESLIADKSGSKKTLRSSLEGPTILDIEKFHRESFFYTHLINFSETLQQCCDLSQLWFREFFLELTMGRRIQ
FPIEMSMPWILTDHILETKEASMMEYVLYSLDLYNDSAHYALTRFNKQFLYDEIEAEVNLCFDQFVYKLADQIFAYYKV
MAGSLLLDKRLRSECKNQGATIHLPPSNRYETLLKQRHVQLLGRSIDLNRLITQRVSAAMYKSLELAIGRFESEDLTSIVEL
DGLLEINRMTHKLLSRYLTLDGFDAMFREANHNVSAPYGRITLHVFWELNYDFLPNYCYNGSTNRFVRTVLPFSQEFQR
DKQPNAQPQYLHGSKALNLAYSSIYGSYRNFVGPPHFQVICRLLGYQGIAVVMEELLKVVKSLLQGTILQYVKTLMEVM
PKICRLPRHEYGSPGILEFFHHQLKDIVEYAELKTVCFQNLREVGNAILFCLLIEQSLSLEEVCDLLHAAPFQNILPRVHVKE
GERLDAKMKRLESKYAPLHLVPLIERLGTPQQIAIAREGDLLTKERLCCGLSMFEVILTRIRSFLDDPIWRGPLPSNGVMH
VDECVEFHRLWSAMQFVYCIPVGTHEFTVEQCFGDGLHWAGCMIIVLLGQQRRFAVLDFCYHLLKVQKHDGKDEIIKNV
PLKKMVERIRKFQILNDEIITILDKYLKSGDGEGTPVEHVRCFQPPIHQSLASS**GGSGGSGGSGGS**MQAIKCVVVGDGAV
GKTCLLISYTTNAF**S**GEYIPTVFDNYSANVMVDGKPVNLGLWDTAG**L**EDYDRLRPLSYPQTDVFLICFSLVSPASFENVR
AKWYPEVRHHCPNTPIILVGTKLDLRDDKDTIEKLKEKKLTPITYPQGLAMAKEIGAVKYLECSALTQRGLKTVFDEAIR
AVLCPPPVKKRKRK

>Nap1
GAMSRSVLQPSQQKLAEKLTILNDRGVGMLTRLYNIKKACGDPKAKPSYLIDKNLESAVKFIVRKFPAVETRNNNQQLA
QLQKEKSEILKNLALYYFTFVDVMEFKDHVCELLNTIDVCQVFFDITVNFDLTKNYLDLIITYTTLMILLSRIEERKAIIGLY
NYAHEMTHGASDREYPRLGQMIVDYENPLKKMMEEFVPHSKSLSDALISLQMVYPRRNLSADQWRNAQLLSLISAPSTM
LNPAQSDTMPCEYLSLDAMEKWIIFGFILCHGILNTDATALNLWKLALQSSSCLSLFRDEVFHIHKAAEDLFVNIRGYNKR
INDIRECKEAAVSHAGSMHRERRKFLRSALKELATVLSDQPGLLGPKALFVFMALSFARDEIIWLLRHADNMPKKSADDF
IDKHIAELIFYMEELRAHVRKYGPVMQRYYVQYLSGFDAVVLNELVQNLSVCPEDESIIMSSFVNTMTSLSVKQVEDGEV
FDFRGMRLDWFRLQAYTSVSKASLGLADHRELGKMMNTIIFHTKMVDSLVEMLVETSDLSIFCFYSRAFEKMFQQCLEL
PSQSRYSIAFPLLCTHFMSCTHELCPEERHHIGDRSLSLCNMFLDEMAKQARNLITDICTEQCTLSDQLLPKHCAKTISQAV
NKKSKKQTGKKGEPEREKPGVESMRKNRLVVTNLDKLHTALSELCFSINYVPNMVVWEHTFTPREYLTSHLEIRFTKSIV
GMTMYNQATQEIAKPSELLTSVRAYMTVLQSIENYVQIDITRVFNNVLLQQTQHLDSHGEPTITSLYTNWYLETLLRQVS
NGHIAYFPAMKAFVNLPTENELTFNAEEYSDISEMRSLSELLGPYGMKFLSESLMWHISSQVAELKKLVVENVDVLTQM
RTSFDKPDQMAALFKRLSSVDSVLKRMTIIGVILSFRSLAQEALRDVLSYHIPFLVSSIEDFKDHIPRETDMKVAMNVYELS
SAAGLPCEIDPALVVALSSQKSENISPEEEYKIACLLMVFVAVSLPTLASNVMSQYSPAIEGHCNNIHCLAKAINQIAAALF
TIHKGSIEDRLKEFLALASSSLLKIGQETDKTTTRNRESVYLLLDMIVQESPFLTMDLLESCFPYVLLRNAYHAVYKQSVTS
SA

>WAVE1 (1-230)
GHMPLVKRNIDPRHLCHTALPRGIKNELECVTNISLANIIRQLSSLSKYAEDIFGELFNEAHSFSFRVNSLQERVDRLSVSVT
QLDPKEEELSLQDITMRKAFRSSTIQDQQLFDRKTLPIPLQETYDVCEQPPPLNILTPYRDDGKEGLKFYTNPSYFFDLWKE
KMLQDTEDKRKEKRKQKQKNLDRPHEPEKVPRAPHDRRREWQKLAQGPELAEDDANLLHKHIEVANG

>WAVE1 (1-230)-WCA, or **WAVE1 (1-230)-(GGS)$_6$-WCA(485-559)**
GHMPLVKRNIDPRHLCHTALPRGIKNELECVTNISLANIIRQLSSLSKYAEDIFGELFNEAHSFSFRVNSLQERVDRLSVSVT
QLDPKEEELSLQDITMRKAFRSSTIQDQQLFDRKTLPIPLQETYDVCEQPPPLNILTPYRDDGKEGLKFYTNPSYFFDLWKE
KMLQDTEDKRKEKRKQKQKNLDRPHEPEKVPRAPHDRRREWQKLAQGPELAEDDANLLHKHIEVANG**GGSGGSGGS
GGSGGSGGS**KRHPSTLPVISDARSVLLEAIRKGIQLRKVEEQREQEAKHERIENDVATILSRRIAVEYSDSEDDSEFDEVD
WLE

>WAVE1 (1-230)-Rac1, or **WAVE1 (1-230)-(GGS)$_6$-Rac1$^{Q61L/P29S}$(1-188)**
GHMPLVKRNIDPRHLCHTALPRGIKNELECVTNISLANIIRQLSSLSKYAEDIFGELFNEAHSFSFRVNSLQERVDRLSVSVT
QLDPKEEELSLQDITMRKAFRSSTIQDQQLFDRKTLPIPLQETYDVCEQPPPLNILTPYRDDGKEGLKFYTNPSYFFDLWKE
KMLQDTEDKRKEKRKQKQKNLDRPHEPEKVPRAPHDRRREWQKLAQGPELAEDDANLLHKHIEVANG**GGSGGSGGS
GGSGGSGGS**MQAIKCVVVGDGAVGKTCLLISYTTNAF**S**GEYIPTVFDNYSANVMVDGKPVNLGLWDTAG**L**EDYDRLR
PLSYPQTDVFLICFSLVSPASFENVRAKWYPEVRHHCPNTPIILVGTKLDLRDDKDTIEKLKEKKLTPITYPQGLAMAKEIG
AVKYLECSALTQRGLKTVFDEAIRAVLCPPPVKKRKRK

>Abi2 (1-158)
GHMAELQMLLEEEIPGGRRALFDSYTNLERVADYCENNYIQSADKQRALEETKAYTTQSLASVAYLINTLANNVLQMLD
IQASQLRRMESSINHISQTVDIHKEKVARREIGILTTNKNTSRTHKIIAPANLERPVRYIRKPIDYTILDDIGHGVKVSTQ

>HSPC300
GHMGAAMAGQEDPVQREIHQDWANREYIEIITSSIKKIADFLNSFDMSCRSRLATLNEKLTALERRIEYIEARVTKGETLT

>WCA
KRHPSTLPVISDARSVLLEAIRKGIQLRKVEEQREQEAKHERIENDVATILSRRIAVEYSDSEDDSEFDEVDWLE

> **GST-Arf1**
MSPILGYWKIKGLVQPTRLLLEYLEEKYEEHLYERDEGDKWRNKKFELGLEFPNLPYYIDGDVKLTQSMAIIRYIADKHN
MLGGCPKERAEISMLEGAVLDIRYGVSRIAYSKDFETLKVDFLSKLPEMLKMFEDRLCHKTYLNGDHVTHPDFMLYDAL
DVVLYMDPMCLDAFPKLVCFKKRIEAIPQIDKYLKSSKYIAWPLQGWQATFGGGDHPPKSDLVPRGS**MRILMVGLDAAG
KTTILYKLKLGEIVTTIPTIGFNVETVEYKNISFTVWDVGGQDKIRPLWRHYFQNTQGLIFVVDSNDRERVNEAREELMRM
LAEDELRDAVLLVFANKQDLPNAMNAAEITDKLGLHSLRHRNWYIQATCATSGDGLYEGLDWLSNQLRNQK**

> **His8-Arf1**
HHHHHHHHGGSGGS**MRILMVGLDAAGKTTILYKLKLGEIVTTIPTIGFNVETVEYKNISFTVWDVGGQDKIRPLWRHYFQ**
NTQGLIFVVDSNDRERVNEAREELMRMLAEDELRDAVLLVFANKQDLPNAMNAAEITDKLGLHSLRHRNWYIQATCAT

SGDGLYEGLDWLSNQLRNQK

> **His6-EspG**
MSYYHHHHHHDYDIPTTENLYFQGAMGSKKSWDEMSCAEKLFKVLSFGLWNPTYSRSERQSFQELLTVLEPVYPLPNEL
GRVSARFSDGSSLRISVTNSELVEAEIRTANNEKITVLLESNEQNRLLQSLPIDRHMPYIQVHRALSEMDLTDTTSMRNLLG
FTSKLSTTLIPHNAQTDPLSGPTPFSSIFMDTCRGLGNAKLSLNGVDIPANAQKLLRDALGLKDTHSSPTRNVIDHGISRHD
AEQIARESSGSDKQKAEVVEFLCHPEAATAICSAFYQSFNVPALTLTHERISKASEYNAERSLDTPNACINISISQSSDGNIY
VTSHTGVLIMAPEDRPNEMGMLTNRTSYEVPQGVKCIIDEMVSALQPRYAASETYLQNT

> **GST-Arf5**
MSPILGYWKIKGLVQPTRLLLEYLEEKYEEHLYERDEGDKWRNKKFELGLEFPNLPYYIDGDVKLTQSMAIIRYIADKHN
MLGGCPKERAEISMLEGAVLDIRYGVSRIAYSKDFETLKVDFLSKLPEMLKMFEDRLCHKTYLNGDHVTHPDFMLYDAL
DVVLYMDPMCLDAFPKLVCFKKRIEAIPQIDKYLKSSKYIAWPLQGWQATFGGGDHPPKSDLVPRGSMRILMVGLDAAG
KTTILYKLKLGEIVTTIPTIGFNVETVEYKNICFTVWDVGGQDKIRPLWRHYFQNTQGLIFVVDSNDRERVQESADELQKM
LQEDELRDAVLLVFANKQDMPNAMPVSELTDKLGLQHLRSRTWYVQATCATQGTGLYDGLDWLSHELSKR

> **GST-Arf6**
MSPILGYWKIKGLVQPTRLLLEYLEEKYEEHLYERDEGDKWRNKKFELGLEFPNLPYYIDGDVKLTQSMAIIRYIADKHN
MLGGCPKERAEISMLEGAVLDIRYGVSRIAYSKDFETLKVDFLSKLPEMLKMFEDRLCHKTYLNGDHVTHPDFMLYDAL
DVVLYMDPMCLDAFPKLVCFKKRIEAIPQIDKYLKSSKYIAWPLQGWQATFGGGDHPPKSDLVPRGSMRILMLGLDAAG
KTTILYKLKLGQSVTTIPTVGFNVETVTYKNVKFNVWDVGGQDKIRPLWRHYYTGTQGLIFVVDCADRDRIDEARQELH
RIINDREMRDAIILIFANKQDLPDAMKPHEIQEKLG LTRIRDRNWYVQPSCATSGDGLYEGLTWLTSNYKS

> **GST-Arl1**
MSPILGYWKIKGLVQPTRLLLEYLEEKYEEHLYERDEGDKWRNKKFELGLEFPNLPYYIDGDVKLTQSMAIIRYIADKHN
MLGGCPKERAEISMLEGAVLDIRYGVSRIAYSKDFETLKVDFLSKLPEMLKMFEDRLCHKTYLNGDHVTHPDFMLYDAL
DVVLYMDPMCLDAFPKLVCFKKRIEAIPQIDKYLKSSKYIAWPLQGWQATFGGGDHPPKSDLVPRGSMRILILGLDGAGK
TTILYRLQVGEVVTTIPTIGFNVETVTYKNLKFQVWDLGGQTSIRPYWRCYYSNTDAVIYVVDSCDRDRIGISKSELVAML
EEEELRKAILVVFANKQDMEQAMTSSEMANSLGLPALKDRKWQIFKTSATKGTGLDEAMEWLVETLKSRQ

> **GST-Arl2**
MSPILGYWKIKGLVQPTRLLLEYLEEKYEEHLYERDEGDKWRNKKFELGLEFPNLPYYIDGDVKLTQSMAIIRYIADKHN
MLGGCPKERAEISMLEGAVLDIRYGVSRIAYSKDFETLKVDFLSKLPEMLKMFEDRLCHKTYLNGDHVTHPDFMLYDAL
DVVLYMDPMCLDAFPKLVCFKKRIEAIPQIDKYLKSSKYIAWPLQGWQATFGGGDHPPKSDLVPRGSERELRLLMLGLD
NAGKTTILKKFNGEDIDTISPTLGFNIKTLEHRGFKLNIWDVGGQKSLRSYWRNYFESTDGLIWVVDSADRQRMQDCQRE
LQSLLVEERLAGATLLIFANKQDLPGALSSNAIREALELDSIRSHHWCIQGCSAVTGENLLPGIDWLLDDISSRIFTAD

>**GST-Rac1^{QP}** or **GST-Tev-Rac1$^{Q61L/P29S}$(1-188)**
MSPILGYWKIKGLVQPTRLLLEYLEEKYEEHLYERDEGDKWRNKKFELGLEFPNLPYYIDGDVKLTQSMAIIRYIADKHN
MLGGCPKERAEISMLEGAVLDIRYGVSRIAYSKDFETLKVDFLSKLPEMLKMFEDRLCHKTYLNGDHVTHPDFMLYDAL
DVVLYMDPMCLDAFPKLVCFKKRIEAIPQIDKYLKSSKYIAWPLQGWQATFGGGDHPPKSDLVPRGSENLYFQGHMQAI
KCVVVGDGAVGKTCLLISYTTNAF**S**GEYIPTVFDNYSANVMVDGKPVNLGLWDTAG**L**EDYDRLRPLSYPQTDVFLICFS
LVSPASFENVRAKWYPEVRHHCPNTPIILVGTKLDLRDDKDTIEKLKEKKLTPITYPQGLAMAKEIGAVKYLECSALTQR
GLKTVFDEAIRAVLCPPPVKKRKRK

>**GST-Rac1^{dead}** or **GST-Tev-Rac1(1-188)**, with Switch I (a.a. 25-39) replaced by **(GGS)$_5$**
MSPILGYWKIKGLVQPTRLLLEYLEEKYEEHLYERDEGDKWRNKKFELGLEFPNLPYYIDGDVKLTQSMAIIRYIADKHN
MLGGCPKERAEISMLEGAVLDIRYGVSRIAYSKDFETLKVDFLSKLPEMLKMFEDRLCHKTYLNGDHVTHPDFMLYDAL
DVVLYMDPMCLDAFPKLVCFKKRIEAIPQIDKYLKSSKYIAWPLQGWQATFGGGDHPPKSDLVPRGSENLYFQGHMQAI
KCVVVGDGAVGKTCLLISYT**GGSGGSGGSGGSGGS**YSANVMVDGKPVNLGLWDTAGQEDYDRLRPLSYPQTDVFLIC
FSLVSPASFENVRAKWYPEVRHHCPNTPIILVGTKLDLRDDKDTIEKLKEKKLTPITYPQGLAMAKEIGAVKYLECSALTQ
RGLKTVFDEAIRAVLCPPPVKKRKRK

> **Rac1^{QP}** or **Rac1$^{Q61L/P29S}$(1-188)**
MQAIKCVVVGDGAVGKTCLLISYTTNAF**S**GEYIPTVFDNYSANVMVDGKPVNLGLWDTAG**L**EDYDRLRPLSYPQTDVF
LICFSLVSPASFENVRAKWYPEVRHHCPNTPIILVGTKLDLRDDKDTIEKLKEKKLTPITYPQGLAMAKEIGAVKYLECSA
LTQRGLKTVFDEAIRAVLCPPPVKKRKRK

842

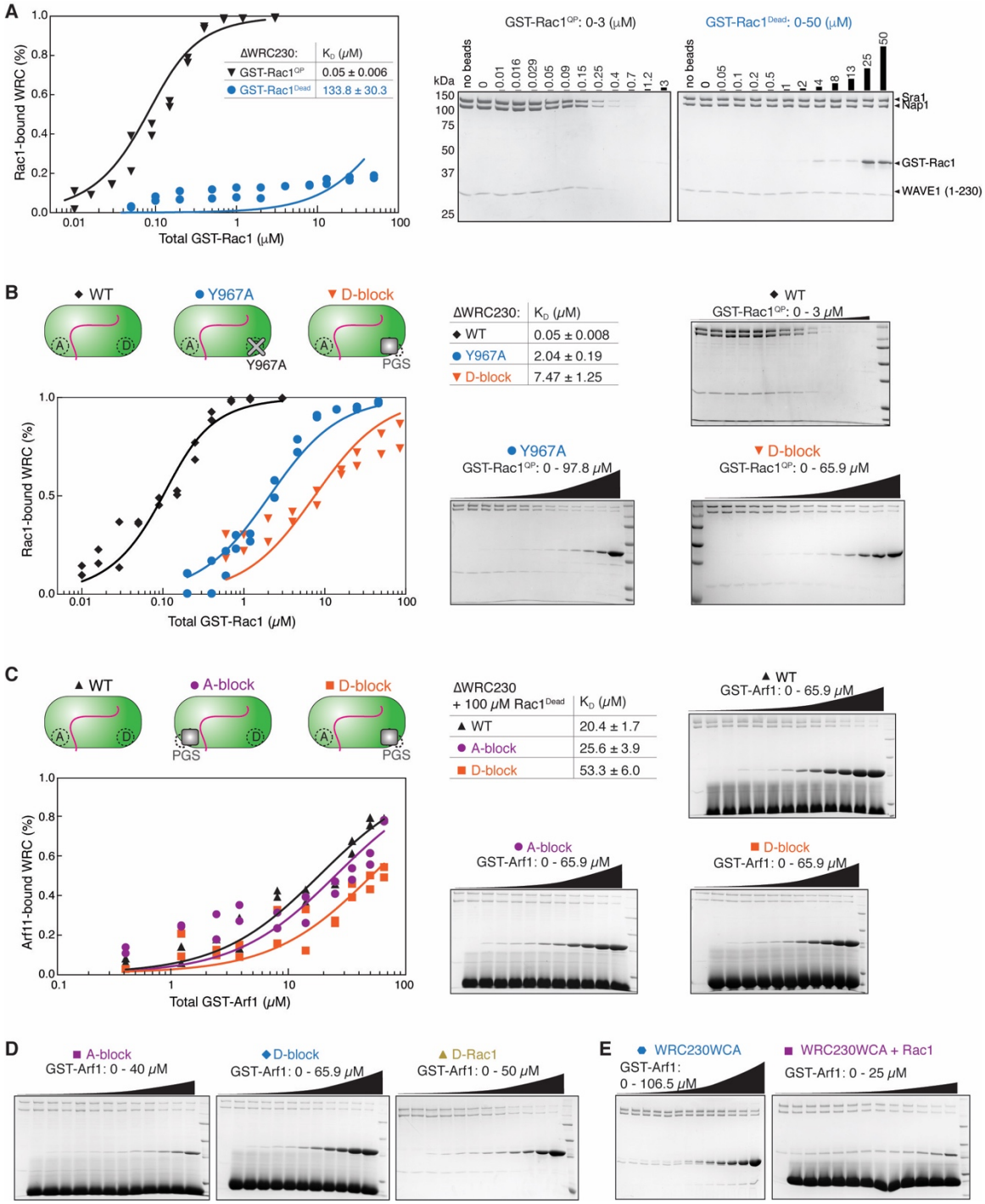

Figure S1. Supporting EDP data for Figures 1, 2, and 3 (Related to Figures 1, 2, and 3). (A) EPD measurement, including quantification and representative Coomassie blue-stained SDS PAGE gels, showing GST-Rac1^{Dead} does bind to WRC. **(B)** EPD measurement showing that, compared to the Y967A mutation, D-block further reduces potential leaky

848 binding of Rac1 to the D site. **(C)** EPD measurement showing that blocking the A site or
849 the D site does not significantly affect the basal level binding of Arf1 to WRC. **(D-E)**
850 Example EPD gels for Figures 2B and 3B, respectively.
851

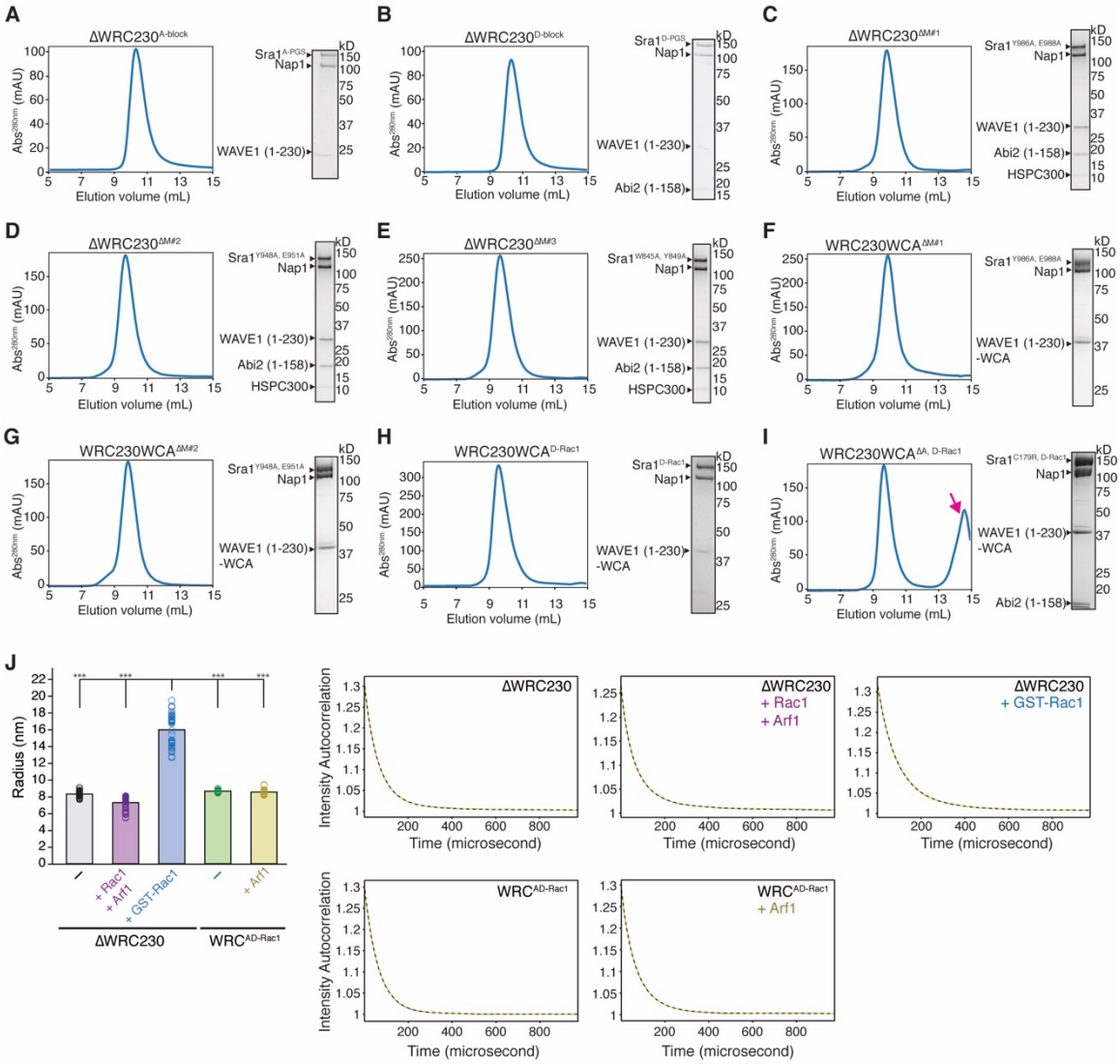

852

853 **Figure S2. Quality control of the WRCs newly developed in this study (Related to**

854 **Figures 1, 2, 3, and 5). (A-I)** Shown are the final steps or analytical steps of WRC

855 purifications using 24-ml Superdex 200 gel filtration columns, with Coomassie blue-

856 stained SDS-PAGE gels showing the peak or pooled fractions. Depending on whether the

857 preceding purification step included a Source Q15 ion exchange column, different amounts

858 of Tev and cleaved MBP tag may show as clearly separated peaks (indicated by magenta

859 arrow) following the WRC peak. **(J)** Dynamic Light Scattering (DLS) measurements of

860 indicated WRC mixed with GTPases. GST-Rac1 is used as a positive control to show

radius change when WRC is dimerized by GST-Rac1. On the left is radius values for 3.3 μM ΔWRC230 alone (n = 54), 3.5 μM ΔWRC230 + 30 μM $Rac1^{QP}$ + 125 μM Arf1 (n = 44), 1 μM ΔWRC230 + 30 μM GST-$Rac1^{QP}$ (n = 51), 5 μM $WRC^{AD\text{-}Rac1}$ alone (n = 16), and 5 μM $WRC^{AD\text{-}Rac1}$ + 125 μM $Rac1^{QP}$ (n = 24). n equals total number of acquisitions, *** indicates $p < 0.001$, ANOVA test. Radius values are reported as the average values from all requisitions. All experiments were collected in 50-100 mM NaCl and 5% (w/v) glycerol and at room temperature. The slightly reduced radius for ΔWRC230 + Rac1 + Arf1 sample was likely due to the addition of large amounts of Rac1 and Arf1, which have lower molecular weight. On the right is a representative plot of intensity autocorrelation (black solid curve) and the regularization fit (yellow dashed curve) for each experiment.

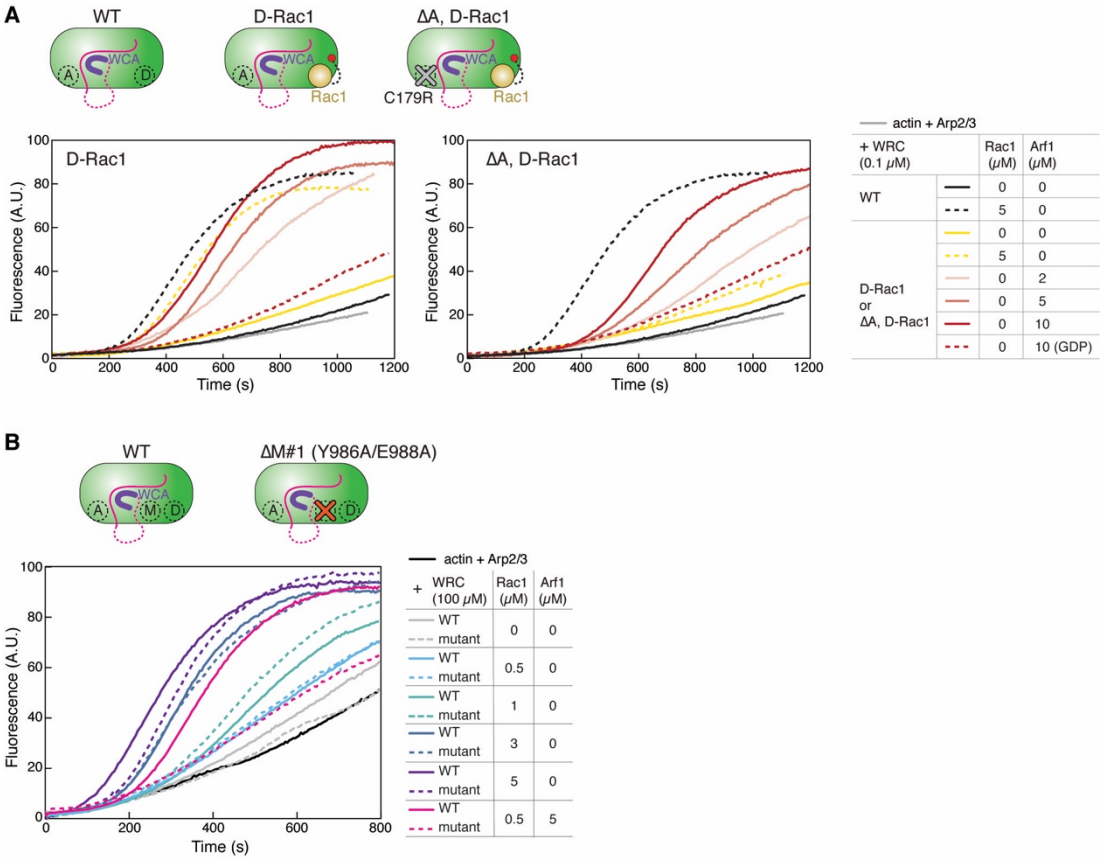

872

873 **Figure S3. Additional actin polymerization assays comparing Arf1- vs. Rac1-**
874 **mediated WRC activation (Related to Figures 3 and 5). (A-B)** Pyrene-actin
875 polymerization assays comparing indicated WRC variants in response to the addition of
876 free Rac1^{QP} or Arf1. WT WRC230WCA was used as a reference point. Reactions
877 contained 3.5 µM actin (5% pyrene labeled), 10 nM Arp2/3 complex, 100 nM indicated
878 WRC, and indicated amounts of Rac1^{QP} and/or Arf1. In all assays, Arf1 is loaded with
879 GNPPNP, unless it is designated with GDP.

880

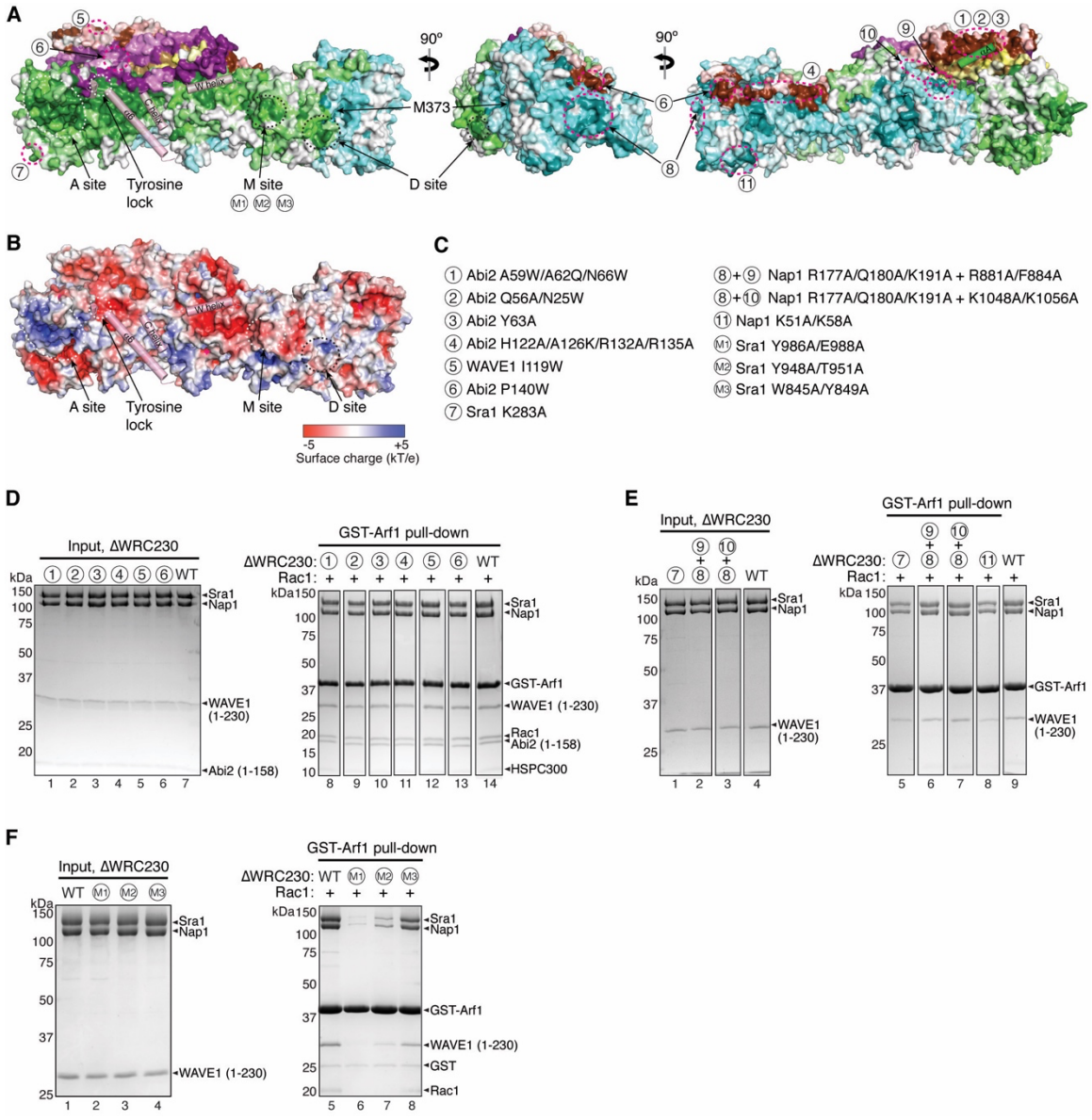

881

882 **Figure S4. Surveying various conserved surfaces on WRC to identify the Arf1-**
883 **binding site (Related to Figures 4 and 5). (A-B)** Surface conservation (A) and
884 electrostatic charge (B) representation of the WRC. (A) was calculated by Consurf
885 (Ashkenazy et al., 2016), and (B) by APBS in Pymol (Jurrus et al., 2018). In (A), color to
886 white gradients represent the most conserved surface residues (ConSurf score = 9 for
887 darkest colors) to the least conserved residues (ConSurf score = 1 for white color).
888 Important sites on Sra1, including the identified Arf1 binding site (M site), are indicated

with white or black dotted circles. Positions of mutations examined in (D-F) are indicated with magenta dotted circles. Semitransparent pink cylinders refer to the sequences in WAVE1 that are destabilized upon WRC activation by Rac1. The αA helix in Sra1 is also shown as a semitransparent green cylinder for clarity. **(C)** Information of the mutations indicated in (A) and examined in (D-F). **(D-F)** Coomassie blue-stained SDS PAGE gels showing GST-Arf1 pull-down of ΔWRC230 carrying indicated surface mutations.

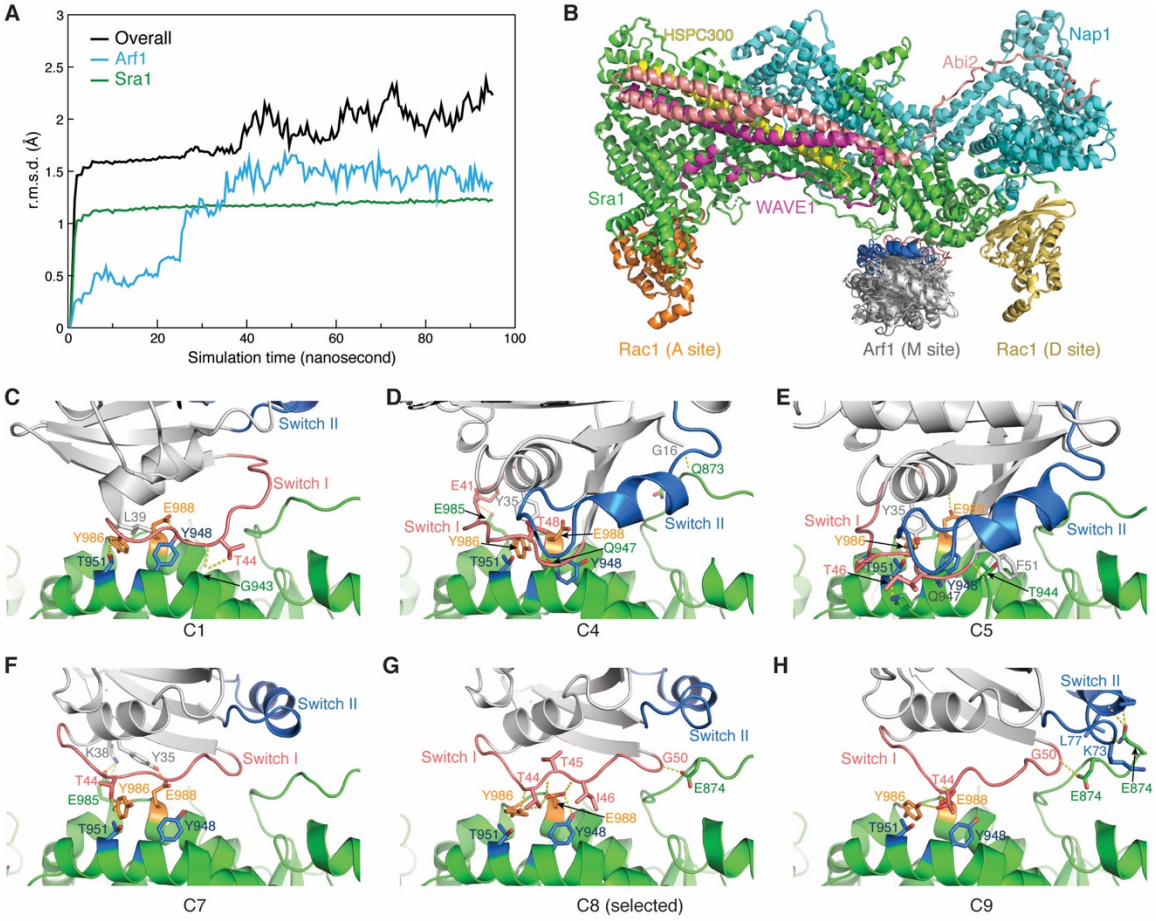

I

System		Free energies of the whole Arf1-WRC$^{AD\text{-}Rac1}$ complex						Free energies of Arf1 binding to WRC$^{AD\text{-}Rac1}$					
model	mutation	E_{vdw}	E_{ele}	G^{sol}_{polar}	$G^{sol}_{nonpolar}$	TS	$G_{MM\text{-}PBSA\text{-}WSAS}$	E_{vdw}	E_{ele}	G^{sol}_{polar}	$G^{sol}_{nonpolar}$	TS	$G_{MM\text{-}PBSA\text{-}WSAS}$
C1	WT	-15569.59±6.45	-25689.81±4.53	-9969.32±0.86	694.41±0.64	35791.12±0.89	-9539.18±11.25	-43.36±0.49	331.84±1.27	-304.51±1.59	-4.25±0.02	-19.57±0.25	-0.71±0.67
	ΔM#1	-15559.76±7.33	-25771.60±0.43	-9873.65±0.13	694.98±0.45	35779.34±1.93	-9531.29±8.63	-39.64±0.92	304.68±1.30	-282.04±1.11	-3.81±0.05	-18.68±0.33	-2.13±0.57
	ΔM#2	-15560.81±7.28	-25674.19±1.04	-9972.81±0.66	694.92±0.45	35782.28±1.89	-9536.06±9.36	-37.64±0.71	332.23±1.20	-306.10±1.05	-3.89±0.04	-18.03±0.30	2.64±0.72
	ΔM#3	-15559.51±7.71	-25682.43±0.95	-9972.47±0.66	694.43±0.44	35774.76±1.83	-9539.69±10.17	-42.54±0.99	332.62±1.15	-305.18±0.99	-4.20±0.03	-19.40±0.34	0.09±0.81
C4	WT	-15532.98±21.22	-25690.78±15.42	-9976.65±13.12	692.84±0.16	35780.95±0.48	-9501.03±24.31	-36.08±0.87	291.85±1.99	-270.47±1.57	-4.13±0.09	-19.03±0.13	0.20±0.51
	ΔM#1	-15519.39±20.84	-25756.19±15.41	-9893.34±13.27	693.32±0.17	35772.16±0.47	-9481.03±24.51	-30.78±0.56	280.67±1.78	-260.83±1.45	-3.72±0.08	-16.30±0.13	1.65±0.27
	ΔM#2	-15521.08±21.51	-25676.08±15.32	-9977.85±13.03	693.18±0.16	35773.25±0.45	-9487.85±24.49	-33.34±0.87	291.96±1.92	-271.27±1.52	-4.05±0.09	-18.35±0.10	1.65±0.54
	ΔM#3	-15519.82±20.99	-25685.88±15.48	-9976.40±13.21	692.88±0.15	35766.18±0.51	-9492.97±24.36	-36.01±0.87	291.93±1.98	-270.52±1.56	-4.13±0.09	-19.03±0.13	0.29±0.51
C5	WT	-15530.30±16.40	-25745.00±6.63	-9918.23±5.24	689.54±0.10	35776.63±1.53	-9503.97±21.48	-65.27±0.77	302.36±0.69	-275.42±0.58	-6.74±0.08	-26.86±0.17	-18.21±0.59
	ΔM#1	-15517.55±16.21	-25816.75±6.39	-9828.87±4.95	690.12±0.08	35766.63±1.44	-9483.19±21.90	-61.05±1.00	287.15±1.01	-261.53±0.84	-6.22±0.07	-25.09±0.19	-16.56±0.69
	ΔM#2	-15519.42±15.86	-25727.59±6.72	-9922.05±5.33	689.94±0.09	35769.63±1.49	-9492.22±22.26	-61.88±0.93	306.56±0.57	-279.82±0.46	-6.56±0.08	-25.19±0.20	-16.52±0.71
	ΔM#3	-15515.32±16.65	-25740.41±6.45	-9917.68±5.14	689.59±0.09	35762.44±1.54	-9494.00±21.19	-64.96±0.73	302.46±0.69	-275.53±0.59	-6.73±0.07	-26.86±0.17	-17.89±0.56
C7	WT	-15542.18±12.06	-25776.00±12.13	-9899.55±11.90	686.19±0.21	35771.98±1.90	-9505.71±26.51	-71.40±0.87	274.46±3.24	-248.44±2.58	-9.08±0.07	-28.28±0.06	-26.19±0.38
	ΔM#1	-15529.34±12.05	-25840.27±12.56	-9815.78±12.19	686.61±0.22	35763.39±2.00	-9487.10±26.59	-66.61±0.74	260.04±3.13	-235.37±2.75	-8.78±0.08	-26.10±0.10	-24.62±0.23
	ΔM#2	-15530.46±12.23	-25759.15±12.23	-9901.94±11.93	686.50±0.22	35765.10±1.89	-9492.07±27.29	-67.61±0.82	274.19±3.22	-248.80±2.55	-9.04±0.07	-27.29±0.05	-23.98±0.41
	ΔM#3	-15528.76±12.19	-25771.69±12.19	-9899.73±12.03	686.28±0.22	35757.17±1.90	-9498.29±26.56	-71.31±0.87	274.56±3.23	-248.51±2.57	-9.08±0.07	-28.28±0.06	-26.06±0.39
C8	**WT**	-15572.61±26.33	-25722.41±14.16	-9942.87±9.72	690.31±0.43	35784.32±1.15	**-9524.61±44.36**	-76.97±1.61	301.80±0.32	-272.67±0.36	-8.93±0.08	-29.31±0.36	**-27.46±1.12**
	ΔM#1	-15557.84±25.88	-25785.51±13.42	-9858.63±9.28	690.65±0.44	35776.05±1.09	**-9502.55±44.63**	-70.33±1.49	292.08±0.42	-261.90±0.26	-8.76±0.10	-26.48±0.41	**-22.43±0.75**
	ΔM#2	-15559.40±26.38	-25707.60±13.89	-9944.34±9.77	690.59±0.44	35777.61±1.10	**-9510.56±43.58**	-72.47±1.28	301.15±0.31	-272.96±0.51	-8.91±0.07	-27.81±0.35	**-25.38±0.67**
	ΔM#3	-15559.55±26.48	-25719.08±14.21	-9942.22±9.81	690.38±0.41	35769.74±1.11	**-9516.65±43.91**	-76.70±1.61	301.83±0.28	-272.80±0.35	-8.89±0.08	-29.30±0.36	**-27.26±1.12**
C9	WT	-15538.55±4.49	-25794.92±11.65	-9876.27±6.87	693.73±0.23	35784.20±0.72	-9438.42±43.10	-50.51±0.68	310.70±1.03	-287.05±1.04	-5.39±0.10	-21.77±0.16	-10.47±0.52
	ΔM#1	-15528.50±4.59	-25864.25±11.53	-9787.16±6.74	694.10±0.21	35774.96±0.66	-9421.61±43.86	-48.91±0.46	293.71±1.18	-270.60±1.19	-5.15±0.10	-20.17±0.21	-10.78±0.27
	ΔM#2	-15526.45±4.44	-25777.97±11.56	-9878.46±6.74	693.97±0.23	35777.26±0.71	-9424.98±43.14	-45.89±0.64	310.47±1.01	-287.38±1.00	-5.39±0.10	-20.69±0.14	-7.49±0.56
	ΔM#3	-15522.34±4.68	-25790.76±11.87	-9876.08±7.08	693.97±0.23	35769.97±0.77	-9426.93±42.75	-49.34±0.60	310.94±1.17	-287.52±1.13	-5.13±0.06	-21.50±0.16	-9.55±0.47

Figure S5. Molecular dynamics simulation and energy minimization of the top M-site Arf1 docking models (Related to Figure 4). (A) Root-mean-square deviation (r.m.s.d.) time course of the MD simulation of the C8 model, showing the system reached equilibrium after 30 nanoseconds. Other models showed similar r.m.s.d. time courses. **(B)**

902 Overlay of all six MD energy minimized models. **(C-H)** Detailed view of the Arf1-M site
903 interactions in indicated models. Sra1 is kept in the same orientation to demonstrate
904 different orientations of Arf1 in various MD models. Yellow dotted lines indicate polar or
905 π-π interactions. **(I)** List of MM-PBSA-WSAS energy terms of whole complex free
906 energies (left) and Arf1-binding free energies (right) of six Arf1-WRC$^{AD\text{-}Rac1}$ complexes,
907 each including the WT WRC and M-site mutants, with ΔM#1 for Sra1$^{Y986A/E988A}$, ΔM#2
908 for Sra1$^{948A/T951A}$, and ΔM#3 for Sra1$^{W845A/Y849A}$ (as a negative control). All energy terms,
909 including E_{vdw} and E_{eel} for the van der Waals and electrostatic interactions, respectively;
910 G^{sol}_{polar} and $G^{sol}_{nonpolar}$ for the polar and nonpolar parts of the solvation free energy,
911 respectively, and TS for the entropic term, are in kcal/mol. Model C8 agreed best with the
912 experimental results, in that ΔM#1 and ΔM#2, but not ΔM#3 mutations, increased by free
913 energies for Arf1 binding.
914

915 **References**

916 Anitei, M., Stange, C., Parshina, I., Baust, T., Schenck, A., Raposo, G., Kirchhausen, T.,
917 and Hoflack, B. (2010). Protein complexes containing CYFIP/Sra/PIR121 coordinate
918 Arf1 and Rac1 signalling during clathrin-AP-1-coated carrier biogenesis at the TGN. Nat.
919 Cell Biol. *12*.

920 Ashkenazy, H., Abadi, S., Martz, E., Chay, O., Mayrose, I., Pupko, T., and Ben-Tal, N.
921 (2016). ConSurf 2016: an improved methodology to estimate and visualize evolutionary
922 conservation in macromolecules. Nucleic Acids Res. *44*.

923 Balasubramanian, N., Scott, D.W., Castle, J.D., Casanova, J.E., and Schwartz, M.A.
924 (2007). Arf6 and microtubules in adhesion-dependent trafficking of lipid rafts. Nat. Cell
925 Biol. *9*.

926 Baust, T., Czupalla, C., Krause, E., Bourel-Bonnet, L., and Hoflack, B. (2006). Proteomic
927 analysis of adaptor protein 1A coats selectively assembled on liposomes. Proc. Natl.
928 Acad. Sci. U. S. A. *103*.

929 Boshans, R.L., Szanto, S., van Aelst, L., and D'Souza-Schorey, C. (2000). ADP-
930 Ribosylation Factor 6 Regulates Actin Cytoskeleton Remodeling in Coordination with
931 Rac1 and RhoA. Mol. Cell. Biol. *20*.

932 Case, D.A., Walker, R.C., Cheatham, T.E., Simmerling, C., Roitberg, A., Merz, K.M.,
933 Luo, R., and Darden, T. (2018). Amber 2018. Univ. California, San Fr. 2018.

934 Chen, B., Padrick, S.B., Henry, L., and Rosen, M.K. (2014a). Biochemical reconstitution
935 of the WAVE regulatory complex. Methods Enzymol. *540*, 55–72.

936 Chen, B., Brinkmann, K., Chen, Z., Pak, C.W., Liao, Y., Shi, S., Henry, L., Grishin, N.
937 V., Bogdan, S., and Rosen, M.K. (2014b). The WAVE regulatory complex links diverse

938 receptors to the actin cytoskeleton. Cell *156*, 195–207.

939 Chen, B., Chou, H.T., Brautigam, C.A., Xing, W., Yang, S., Henry, L., Doolittle, L.K.,

940 Walz, T., and Rosen, M.K. (2017). Rac1 GTPase activates the WAVE regulatory

941 complex through two distinct binding sites. Elife *6*.

942 Chen, E.H., Pryce, B.A., Tzeng, J.A., Gonzalez, G.A., and Olson, E.N. (2003). Control of

943 myoblast fusion by a guanine nucleotide exchange factor, loner, and its effector ARF6.

944 Cell *114*.

945 Chen, X.J., Squarr, A.J., Stephan, R., Chen, B., Higgins, T.E., Barry, D.J., Martin, M.C.,

946 Rosen, M.K., Bogdan, S., and Way, M. (2014c). Ena/VASP proteins cooperate with the

947 WAVE complex to regulate the actin cytoskeleton. Dev. Cell *30*, 569–584.

948 Chen, Z., Borek, D., Padrick, S.B., Gomez, T.S., Metlagel, Z., Ismail, A.M., Umetani, J.,

949 Billadeau, D.D., Otwinowski, Z., and Rosen, M.K. (2010). Structure and Control of the

950 Actin Regulatory WAVE Complex. Nature *468*, 533–538.

951 Cheng, A., Arumugam, T. V., Liu, D., Khatri, R.G., Mustafa, K., Kwak, S., Ling, H.P.,

952 Gonzales, C., Xin, O., Jo, D.G., et al. (2007). Pancortin-2 interacts with WAVE1 and

953 Bcl-xL in a mitochondria-associated protein complex that mediates ischemic neuronal

954 death. J. Neurosci. *27*.

955 Cook, S.A., Comrie, W.A., Poli, M.C., Similuk, M., Oler, A.J., Faruqi, A.J., Kuhns, D.B.,

956 Yang, S., Vargas-Hernández, A., Carisey, A.F., et al. (2020). HEM1 deficiency disrupts

957 mTORC2 and F-actin control in inherited immunodysregulatory disease. Science (80-.).

958 *369*, 202–207.

959 D'Souza-Schorey, C., and Chavrier, P. (2006). ARF proteins: roles in membrane traffic

960 and beyond. Nat Rev Mol Cell Biol *7*, 347–358.

961 D'Souza-Schorey, C., Boshans, R.L., McDonough, M., Stahl, P.D., and Van Aelst, L.
962 (1997). A role for POR1, a Rac1-interacting protein, in ARF6-mediated cytoskeletal
963 rearrangements. EMBO J. *16*.
964 Derivery, E., Lombard, B., Loew, D., and Gautreau, A. (2009). The Wave complex is
965 intrinsically inactive. Cell Motil. Cytoskelet. *66*, 777–790.
966 Desta, I.T., Porter, K.A., Xia, B., Kozakov, D., and Vajda, S. (2020). Performance and Its
967 Limits in Rigid Body Protein-Protein Docking. Structure *28*.
968 Ding, B., Yang, S., Schaks, M., Liu, Y., Brown, A., Rottner, K., Chowdhury, S., and
969 Chen, B. (2022). Structures reveal a key mechanism of WAVE Regulatory Complex
970 activation by Rac1 GTPase. BioRxiv *[Preprint]*, May 10. doi:
971 https://doi.org/10.1101/2022.05.10.49.
972 Donaldson, J.G., and Jackson, C.L. (2011). ARF family G proteins and their regulators:
973 Roles in membrane transport, development and disease. Nat. Rev. Mol. Cell Biol.
974 Dong, N., Zhu, Y., Lu, Q., Hu, L., Zheng, Y., and Shao, F. (2012). Structurally distinct
975 bacterial TBC-like GAPs link Arf GTPase to Rab1 inactivation to counteract host
976 defenses. Cell.
977 Doolittle, L.K., Rosen, M.K., and Padrick, S.B. (2013). Measurement and analysis of in
978 vitro actin polymerization. Methods Mol Biol *1046*, 273–293.
979 Eden, S., Rohatgi, R., Podtelejnikov, A. V., Mann, M., and Kirschner, M.W. (2002).
980 Mechanism of regulation of WAVE1-induced actin nucleation by Rac1 and Nck. Nature
981 *418*, 790–793.
982 Etienne-Manneville, S., and Hall, A. (2002). Rho GTPases in cell biology. Nature *420*.
983 Gautreau, A., Ho, H.Y.H., Li, J., Steen, H., Gygi, S.P., and Kirschner, M.W. (2004).

Purification and architecture of the ubiquitous Wave complex. Proc. Natl. Acad. Sci. U. S. A. *101*.

Gillingham, A.K., and Munro, S. (2007). The small G proteins of the Arf family and their regulators. Annu. Rev. Cell Dev. Biol. *23*.

Honda, A., Nogami, M., Yokozeki, T., Yamazaki, M., Nakamura, H., Watanabe, H., Kawamoto, K., Nakayama, K., Morris, A.J., Frohman, M.A., et al. (1999). Phosphatidylinositol 4-phosphate 5-kinase α is a downstream effector of the small G protein ARF6 in membrane ruffle formation. Cell *99*.

Hu, B., Shi, B., Jarzynka, M.J., Yiin, J.J., D'Souza-Schorey, C., and Cheng, S.Y. (2009). ADP-ribosylation factor 6 regulates glioma cell invasion through the IQ-domain GTPase-activating protein 1-Rac1-mediated pathway. Cancer Res. *69*.

Humphreys, D., Liu, T., Davidson, A.C., Hume, P.J., and Koronakis, V. (2012a). The Drosophila Arf1 homologue Arf79F is essential for lamellipodium formation. J Cell Sci *125*, 5630–5635.

Humphreys, D., Davidson, A., Hume, P.J., and Koronakis, V. (2012b). Salmonella virulence effector SopE and Host GEF ARNO cooperate to recruit and activate WAVE to trigger bacterial invasion. Cell Host Microbe *11*, 129–139.

Humphreys, D., Davidson, A.C., Hume, P.J., Makin, L.E., and Koronakis, V. (2013). Arf6 coordinates actin assembly through the WAVE complex, a mechanism usurped by Salmonella to invade host cells. Proc Natl Acad Sci U S A *110*, 16880–16885.

Humphreys, D., Singh, V., and Koronakis, V. (2016). Inhibition of WAVE Regulatory Complex Activation by a Bacterial Virulence Effector Counteracts Pathogen Phagocytosis. Cell Rep *17*, 697–707.

1007 Hunt, E.L., Rai, H., and Harris, T.J.C. (2022). SCAR/WAVE complex recruitment to a
1008 supracellular actomyosin cable by myosin activators and a junctional Arf-GEF during
1009 Drosophila dorsal closure. Mol. Biol. Cell.
1010 Ismail, A.M., Padrick, S.B., Chen, B., Umetani, J., and Rosen, M.K. (2009). The WAVE
1011 Regulatory Complex is Inhibited. Nat. Struct. Mol. Biol. *16*, 561–563.
1012 Jurrus, E., Engel, D., Star, K., Monson, K., Brandi, J., Felberg, L.E., Brookes, D.H.,
1013 Wilson, L., Chen, J., Liles, K., et al. (2018). Improvements to the APBS biomolecular
1014 solvation software suite. Protein Sci. *27*.
1015 Kang, R., Tang, D., Yu, Y., Wang, Z., Hu, T., Wang, H., and Cao, L. (2010). WAVE1
1016 regulates Bcl-2 localization and phosphorylation in leukemia cells. Leukemia *24*.
1017 Kim, P., Li, H., Wang, J., and Zhao, Z. (2021). Landscape of drug-resistance mutations in
1018 kinase regulatory hotspots. Brief. Bioinform. *22*.
1019 Koo, T.H., Eipper, B.A., and Donaldson, J.G. (2007). Arf6 recruits the Rac GEF Kalirin
1020 to the plasma membrane facilitating Rac activation. BMC Cell Biol. *8*.
1021 Koronakis, V., Hume, P.J., Humphreys, D., Liu, T., Hørning, O., Jensen, O.N., and
1022 McGhie, E.J. (2011). WAVE regulatory complex activation by cooperating GTPases Arf
1023 and Rac1. Proc. Natl. Acad. Sci. U. S. A. *108*, 14449–14454.
1024 Krauss, M., Kinuta, M., Wenk, M.R., De Camilli, P., Takei, K., and Haucke, V. (2003).
1025 ARF6 stimulates clathrin/AP-2 recruitment to synaptic membranes by activating
1026 phosphatidylinositol phosphate kinase type Iγ. J. Cell Biol. *162*.
1027 Lebensohn, A.M., and Kirschner, M.W. (2009). Activation of the WAVE complex by
1028 coincident signals controls actin assembly. Mol. Cell *36*, 512.
1029 Lewis-Saravalli, S., Campbell, S., and Claing, A. (2013). ARF1 controls Rac1 signaling

1030 to regulate migration of MDA-MB-231 invasive breast cancer cells. Cell Signal *25*,
1031 1813–1819.
1032 Li, L., Li, C., Sarkar, S., Zhang, J., Witham, S., Zhang, Z., Wang, L., Smith, N., Petukh,
1033 M., and Alexov, E. (2012). DelPhi: a comprehensive suite for DelPhi software and
1034 associated resources. BMC Biophys. *5*.
1035 Maier, J.A., Martinez, C., Kasavajhala, K., Wickstrom, L., Hauser, K.E., and
1036 Simmerling, C. (2015). ff14SB: Improving the Accuracy of Protein Side Chain and
1037 Backbone Parameters from ff99SB. J. Chem. Theory Comput. *11*.
1038 Marchesin, V., Montagnac, G., and Chavrier, P. (2015). ARF6 promotes the formation of
1039 Rac1 and WAVE-dependent ventral F-actin rosettes in breast cancer cells in response to
1040 epidermal growth factor. PLoS One *10*, e0121747.
1041 Mosaddeghzadeh, N., and Ahmadian, M.R. (2021). The rho family gtpases: Mechanisms
1042 of regulation and signaling. Cells *10*.
1043 Myers, K.R., and Casanova, J.E. (2008). Regulation of actin cytoskeleton dynamics by
1044 Arf-family GTPases. Trends Cell Biol. *18*.
1045 Padrick, S.B., Cheng, H.C., Ismail, A.M., Panchal, S.C., Doolittle, L.K., Kim, S., Skehan,
1046 B.M., Umetani, J., Brautigam, C.A., Leong, J.M., et al. (2008). Hierarchical Regulation
1047 of WASP/WAVE Proteins. Mol. Cell *32*, 426–438.
1048 Palacios, F., Schweitzer, J.K., Boshans, R.L., and D'Souza-Schorey, C. (2002). ARF6-
1049 GTP recruits Nm23-H1 to facilitate dynamin-mediated endocytosis during adherens
1050 junctions disassembly. Nat. Cell Biol. *4*.
1051 Phuyal, S., and Farhan, H. (2019). Multifaceted Rho GTPase Signaling at the
1052 Endomembranes. Front. Cell Dev. Biol. *7*.

1053 Pollard, T.D. (2010). A guide to simple and informative binding assays. Mol Biol Cell
1054 *21*, 4061–4067.
1055 Quignot, C., Rey, J., Yu, J., Tufféry, P., Guerois, R., and Andreani, J. (2018).
1056 InterEvDock2: An expanded server for protein docking using evolutionary and biological
1057 information from homology models and multimeric inputs. Nucleic Acids Res. *46*.
1058 Radhakrishna, H., Al-Awar, O., Khachikian, Z., and Donaldson, J.G. (1999). ARF6
1059 requirement for Rac ruffling suggests a role for membrane trafficking in cortical actin
1060 rearrangements. J. Cell Sci. *112*.
1061 Ramírez-Aportela, E., López-Blanco, J.R., and Chacón, P. (2016). FRODOCK 2.0: Fast
1062 protein-protein docking server. Bioinformatics *32*.
1063 Ren, X., Farías, G.G., Canagarajah, B.J., Bonifacino, J.S., and Hurley, J.H. (2013).
1064 Structural basis for recruitment and activation of the AP-1 clathrin adaptor complex by
1065 Arf1. Cell *152*.
1066 Rocchia, W., Alexov, E., and Honig, B. (2001). Extending the applicability of the
1067 nonlinear Poisson-Boltzmann equation: Multiple dielectric constants and multivalent
1068 ions. J. Phys. Chem. B *105*.
1069 Rottner, K., Stradal, T.E.B., and Chen, B. (2021). WAVE regulatory complex. Curr. Biol.
1070 *31*, R512–R517.
1071 Santy, L.C., and Casanova, J.E. (2001). Activation of ARF6 by ARNO stimulates
1072 epithelial cell migration through downstream activation of both Rac1 and phospholipase
1073 D. J. Cell Biol. *154*.
1074 Santy, L.C., Ravichandran, K.S., and Casanova, J.E. (2005). The DOCK180/Elmo
1075 complex couples ARNO-mediated Arf6 activation to the downstream activation of Rac1.

Curr. Biol. *15*.

Schaks, M., Singh, S.P., Kage, F., Thomason, P., Klünemann, T., Steffen, A., Blankenfeldt, W., Stradal, T.E., Insall, R.H., and Rottner, K. (2018). Distinct Interaction Sites of Rac GTPase with WAVE Regulatory Complex Have Non-redundant Functions in Vivo. Curr. Biol. *28*.

Schaks, M., Reinke, M., Witke, W., and Rottner, K. (2020). Molecular Dissection of Neurodevelopmental Disorder-Causing Mutations in CYFIP2. Cells *9*.

Schneider, C.A., Rasband, W.S., and Eliceiri, K.W. (2012). NIH Image to ImageJ: 25 years of image analysis. Nat. Methods *9*.

Singh, V., Davidson, A.C., Hume, P.J., Humphreys, D., and Koronakis, V. (2017). Arf GTPase interplay with Rho GTPases in regulation of the actin cytoskeleton. Small GTPases 0.

Singh, V., Davidson, A.C., Hume, P.J., Humphreys, D., and Koronakis, V. (2019). Arf GTPase interplay with Rho GTPases in regulation of the actin cytoskeleton. Small GTPases *10*, 411–418.

Singh, V., Davidson, A.C., Hume, P.J., and Koronakis, V. (2020). Arf6 can trigger wave regulatory complex-dependent actin assembly independent of arno. Int. J. Mol. Sci. *21*.

Steffen, A., Rottner, K., Ehinger, J., Innocenti, M., Scita, G., Wehland, J., and Stradal, T.E.B. (2004). Sra-1 and Nap1 link Rac to actin assembly driving lamellipodia formation. EMBO J. *23*.

Su, L., Wang, Y., Wang, J., Mifune, Y., Morin, M.D., Jones, B.T., Moresco, E.M.Y., Boger, D.L., Beutler, B., and Zhang, H. (2019). Structural Basis of TLR2/TLR1 Activation by the Synthetic Agonist Diprovocim. J. Med. Chem. *62*.

1099 Sung, J.Y., Engmann, O., Teylan, M.A., Nairn, A.C., Greengard, P., and Kim, Y. (2008).
1100 WAVE1 controls neuronal activity-induced mitochondrial distribution in dendritic
1101 spines. Proc. Natl. Acad. Sci. U. S. A. *105*.
1102 Sztul, E., Chen, P.W., Casanova, J.E., Cherfils, J., Dacks, J.B., Lambright, D.G., Lee,
1103 F.J.S., Randazzo, P.A., Santy, L.C., Schürmann, A., et al. (2019). Arf GTPases and their
1104 GEFs and GAPS: Concepts and challenges. Mol. Biol. Cell *30*.
1105 Takenawa, T., and Suetsugu, S. (2007). The WASP-WAVE protein network: Connecting
1106 the membrane to the cytoskeleton. Nat. Rev. Mol. Cell Biol. *8*, 37–48.
1107 Tarricone, C., Xiao, B., Justin, N., Walker, P.A., Rittinger, K., Gamblin, S.J., and
1108 Smerdon, S.J. (2001). The structural basis of Arfaptin-mediated cross-talk between Rac
1109 and Arf signalling pathways. Nature *411*.
1110 Thompson, J.D., Higgins, D.G., and Gibson, T.J. (1994). CLUSTAL W: Improving the
1111 sensitivity of progressive multiple sequence alignment through sequence weighting,
1112 position-specific gap penalties and weight matrix choice. Nucleic Acids Res. *22*.
1113 Wang, J., and Hou, T. (2012). Develop and test a solvent accessible surface area-based
1114 model in conformational entropy calculations. J. Chem. Inf. Model. *52*.
1115 Wang, E., Sun, H., Wang, J., Wang, Z., Liu, H., Zhang, J.Z.H., and Hou, T. (2019). End-
1116 Point Binding Free Energy Calculation with MM/PBSA and MM/GBSA: Strategies and
1117 Applications in Drug Design. Chem. Rev. *119*.
1118 Wang, J., Wolf, R.M., Caldwell, J.W., Kollman, P.A., and Case, D.A. (2004).
1119 Development and testing of a general Amber force field. J. Comput. Chem. *25*.
1120 Wang, J., Hou, T., and Xu, X. (2006). Recent Advances in Free Energy Calculations with
1121 a Combination of Molecular Mechanics and Continuum Models. Curr. Comput. Aided-

Drug Des. *2*.

Wennerberg, K., Rossman, K.L., and Der, C.J. (2005). The Ras superfamily at a glance. J. Cell Sci. *118*.

Yan, Y., Tao, H., He, J., and Huang, S.Y. (2020). The HDOCK server for integrated protein–protein docking. Nat. Protoc. *15*.

Yin, J., Mobarec, J.C., Kolb, P., and Rosenbaum, D.M. (2015). Crystal structure of the human OX2 orexin receptor bound to the insomnia drug suvorexant. Nature *519*.

Yin, J., Babaoglu, K., Brautigam, C.A., Clark, L., Shao, Z., Scheuermann, T.H., Harrell, C.M., Gotter, A.L., Roecker, A.J., Winrow, C.J., et al. (2016). Structure and ligand-binding mechanism of the human OX 1 and OX 2 orexin receptors. Nat. Struct. Mol. Biol. *23*.

Zhang, Y., He, X., Zhai, J., Ji, B., Man, V.H., and Wang, J. (2021). In silico binding profile characterization of SARS-CoV-2 spike protein and its mutants bound to human ACE2 receptor. Brief. Bioinform. *22*.

Zou, W., Dong, X., Broederdorf, T.R., Shen, A., Kramer, D.A., Shi, R., Liang, X., Miller, D.M., Xiang, Y.K., Yasuda, R., et al. (2018). A Dendritic Guidance Receptor Complex Brings Together Distinct Actin Regulators to Drive Efficient F-Actin Assembly and Branching. Dev. Cell *45*, 362-375.e3.

Van Zundert, G.C.P., Rodrigues, J.P.G.L.M., Trellet, M., Schmitz, C., Kastritis, P.L., Karaca, E., Melquiond, A.S.J., Van Dijk, M., De Vries, S.J., and Bonvin, A.M.J.J. (2016). The HADDOCK2.2 Web Server: User-Friendly Integrative Modeling of Biomolecular Complexes. J. Mol. Biol. *428*.